CHEMICAL LANGUAGE MODELS FOR NATURAL PRODUCTS: A STATE-SPACE MODEL APPROACH

Anonymous authors

000

001

002003004

010 011

012

013

014

016

017

018

019

021

023

025

026

027

028

029

031

034

043 044

045

046

047

048

051

052

Paper under double-blind review

ABSTRACT

Language models are increasingly applied in scientific domains such as chemistry, where chemical language models (CLMs) are well-established for predicting molecular properties or generating de novo compounds for small molecules. However, Natural Products (NPs)—such as penicillin, morphine, and quinine, which have driven major breakthroughs in medicine—have received limited attention in CLM research. This gap limits the potential of NPs as a source of new therapeutics. To bridge this gap, we develop Natural Product-specific CLMs (NPCLMs) by pre-training the latest state-space model variants, Mamba and Mamba-2, which have shown great potential in modeling information-dense sequences, and compare them with transformer baselines (GPT). Using the largest known collection of \sim 1M NPs, we provide the first extensive experimental comparison of selective state-space models (S6) and transformers in NP-focused tasks, along with a comparison of eight tokenization strategies, including character-level, Atomin-SMILES (AIS), general byte-pair encoding (BPE) and NP-specific byte-pair encoding (NPBPE). Model performance is evaluated on two tasks: molecule generation, measured by validity, uniqueness, and novelty, and property prediction (peptide membrane permeability, taste, and anti-cancer activity), evaluated using Matthews Correlation Coefficient (MCC) and Area Under the Receiver Operating Characteristic Curve (AUC-ROC). The results show that Mamba consistently generates 1–2% more valid and unique molecules than Mamba-2 and GPT, while making 3-6% less long-range dependency errors; however, GPT produces $\sim 2\%$ more novel structures. In property prediction, both Mamba and Mamba-2 outperform GPT by a modest but consistent 0.02 to 0.04 improvement in MCC under random splitting. Under stricter scaffold splitting, which groups molecules by core structure to better assess generalization to new scaffolds, all models perform comparably. In addition, chemically informed tokenization further enhances performance. For comparison, we include general-domain CLMs (ChemBERTa-2 and MoLFormer) and found that pre-training on \sim 1M NPs achieves results on par with general CLMs trained on datasets over 100 times larger, emphasizing the value of domain-specific pre-training and data quality over scale in chemical language modeling.

1 Introduction

Natural Products (NPs) are compounds naturally produced by living organisms. Their structural diversity and bioactivity make them particularly valuable candidates for drug discovery (Firn, 2009; Dias et al., 2012; Ertl & Schuffenhauer, 2008). Unlike the common use of 'natural products' to describe plant-based or unmodified consumer goods, here 'NPs' specifically refer to chemical compounds (e.g., caffeine, morphine, and quinine) synthesized by living organisms with ecological or therapeutic relevance. NPs occupy a distinct chemical space shaped by evolution, optimized for biological interaction, and rich in scaffolds rarely found in synthetic compounds (Firn, 2009). Nearly one-fourth of approved drugs between 1981 and 2014 originated from — or were inspired by — NPs, particularly for treating cancer, infectious diseases, and diabetes (Newman & Cragg, 2016). Despite a historical surge in NP discovery, the field has stagnated due to their synthetic complexity, unknown binding targets, and regulatory challenges; however, the potential of NPs in drug discovery

continues to drive interest in new computational methods to explore their largely uncharted chemical space (Harvey et al., 2015; Pye et al., 2017; Saldívar-González et al., 2022).

Advances in artificial intelligence, particularly deep learning and Natural Language Processing (NLP), have enabled new approaches to modeling chemical structures. Representations like SMILES (Simplified Molecular Input Line Entry System) also allow molecules to be treated as text, forming the foundation of CLMs (Weininger, 1988). It is important to note that macromolecules like proteins and DNA have dedicated models and representations. CLMs handle small to medium molecules and their explicit chemical structure in terms of atoms as the basic unit of modelling. CLMs have shown success in molecular generation and property prediction, initially using recurrent architectures like long short-term memory (LSTM) and more recently, transformers (Saldívar-González et al., 2022). Transformers offer strong performance via self-attention but suffer from quadratic complexity, limiting their efficiency on longer or information-dense sequences (Bran & Schwaller, 2024; Bajorath, 2023; Sultan et al., 2024; Jablonka et al., 2024; Vaswani et al., 2017; Tay et al., 2022).

To the best of our knowledge, until now, only causal models, such as GPT, LSTM, and, more recently, structured state-space sequence models (S4), have been applied to NP tasks. We aim to further explore state-space models (SSMs), motivated by prior findings that suggest their superior ability to model complex molecular properties for de novo design compared to GPT (Özçelik et al., 2024). Specifically, we investigate the most recent variants of SSMs, Mamba and Mamba-2, namely selective SSM (S6), that attend to input elements "selectively" over time (Gu & Dao, 2024). Unlike transformers, Mamba process sequences through latent dynamical systems instead of pairwise attention, and they have demonstrated strong performance on a range of sequence modeling tasks, suggesting their potential to effectively capture the complex structural dependencies present in NP molecules (Gu & Dao, 2024; Brazil et al., 2024; Xu et al., 2024; Thoutam & Ellsworth, 2024; Sgarbossa et al., 2024; Peng et al., 2024). NPs are structurally more complex and information-dense than fully synthetic molecules (Firn, 2009; Ertl et al., 2008; Chen et al., 2022; Özçelik et al., 2024; Stahura et al., 2000; Godden & Bajorath, 2001). For instance, Stratton et al. (2015) reported that approved NP drugs average 4.1 nitrogen and 9.3 oxygen atoms per molecule, compared to 2.4 and 2.6 in fully synthetic drugs. NPs also show greater structural complexity, with 8.2 stereocenters and 11 rotatable bonds on average, versus 0.8 and 5.2 in synthetic drugs, underscoring their richer topological and functional diversity. In addition, compared to natural languages, chemical languages lack punctuation and stop words, thus encoding more information per token, which poses more modeling challenges (Ucak et al., 2023).

We use NPs as a case study to probe into selective SSMs versus transformers in modeling dense symbolic sequences, raising hypotheses that may extend beyond chemistry. To this end, we pretrain models from scratch on the largest collection of unique NPs to date, without augmentation by SMILES enumeration, and benchmark Mamba variants against widely used GPT models to address three key questions: (1) Do Mamba models outperform transformer baselines in NP generation and property prediction? (2) Which tokenization strategies are most effective for these tasks? (3) Does fine-tuning CLMs pre-trained on larger and more generic datasets outperform NP-only pre-training? In doing so, we aim to uncover how model type, tokenization, and data-splitting protocols influence model performance on NP sequence processing, while providing reproducible benchmarks and practical insights for future empirical research in this domain.

2 RELATED WORK

Most current CLMs are transformer-based and pre-trained on large molecular databases like ZINC (version 22; ~55B molecules), PubChem (~119M), and ChEMBL (~2.5M), with the latter two focused on experimentally characterized compounds (Liao et al., 2024; Bran & Schwaller, 2024; Sultan et al., 2024). These databases mostly contain small molecules, which include natural, semi-synthetic, and synthetic compounds. Despite the importance of NPs in drug discovery, only a few CLMs are explicitly developed for them. Existing NP-focused CLMs often use transformer or recurrent architectures, and more recently S4. They have mostly been trained on datasets like COCONUT, an open-access collection of approximately 700K NPs, and augmented with SMILES enumeration (a technique that generates multiple valid SMILES strings for the same molecule) to generate NP-like molecules (Shen et al., 2024; Sakano et al., 2024; Tay et al., 2023; Özçelik et al., 2024). These

studies show that large language models (LLMs) can effectively generate NP-like molecules. However, no research has yet applied the latest SSMs variants, Mamba and Mamba-2, to NP-focused CLMs or thoroughly investigated tokenization strategies for NPs. This work aims to address these gaps.

3 METHODOLOGY

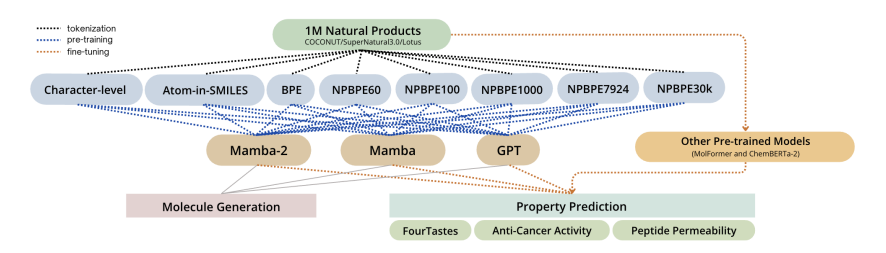


Figure 1: Workflow overview.

3.1 DATA

Pre-training data used in this study is a curated dataset of 1,030,273 NP SMILES (later referred to as 1M NPs) collected from SuperNatural 3.0, COCONUT, and LOTUS, publicly available databases that compile NPs from commercial sources, open-access repositories, and curated literature (Gallo et al., 2022; Sorokina et al., 2021; Rutz et al., 2022). Duplicate molecules were removed, and the ones flagged by RDKit¹ for the following structural issues were also eliminated: explicit valence issues, kekulization problems, sanitization errors, ambiguous stereochemistry, and hydrogen atoms without neighbors. Subsequently, the remaining SMILES strings in the dataset were standardized and canonicalized using RDKit's rdMolStandardize² module to remove small fragments, normalize functional groups, and reionize molecules. Charge neutralization is then applied to adjust charged species, followed by tautomer canonicalization to ensure consistent tautomeric forms.

Downstream data includes three classification datasets: (1) **Peptide membrane permeability** contains 6,651 cyclic natural peptides with binary membrane permeability labels, curated from CycPeptMPDB using PAMPA assay data (Feller & Wilke, 2025; Li et al., 2023a). (2) **FourTastes** includes 4,431 compounds labeled with one of four classes: "sweet," "bitter," "umami," or "other," curated from ChemTastesDB, UMP442, and other literature (Androutsos et al., 2024). (3) **Anticancer activity** consists of ~26,000 compounds with binary labels for general anti-cancer activity, based on growth inhibition data from the NCI-60 screening program (Li & Huang, 2012; Al-Jarf et al., 2021).

All overlapping molecules between 1M NPs and the downstream data have been removed, and all downstream data underwent the same preprocessing as the 1M NPs. Table 5 and Figure 9 in the Appendix show downstream task dataset size, class, and feature distributions. These three datasets were chosen because peptides represent a subset of NPs, while the other two capture common biological roles of NPs, such as shaping taste and smell perception and serving as a rich source of anti-cancer agents (Firn, 2009). Therefore, FourTastes and anti-cancer activity contain a relatively high proportion of NP molecules, although they are not composed exclusively of NPs. Purely NP-specific datasets are either not publicly available or have not been established, primarily due to the high costs associated with conducting assays on a sufficiently large number of NPs necessary for machine learning applications (see Appendix A.3.2 for details).

3.2 Model

The Mamba model used in this study is the MambaLMHeadModel³, a wrapper around the Mamba architecture with a language modeling head. Both Mamba and Mamba-2 share the same overall

¹https://www.rdkit.org/

 $^{^2}$ https://www.rdkit.org/docs/source/rdkit.Chem.MolStandardize.rdMolStandardize.html

https://github.com/state-spaces/mamba/blob/main/mamba_ssm/models/mixer_seq_simple.py#L215

architecture and differ only in the mixer component. The main difference between Mamba and Mamba-2's neural network architecture is that the SSM parameters in Mamba-2 are produced in parallel with the input instead of sequentially as in Mamba (Dao & Gu, 2024). The generative pretrained transformer (GPT) model used in this study is GPT2LMHeadModel ⁴. It is a decoder-only model with a language modeling head from the GPT-2 family. All models are pre-trained from scratch on A100 GPUs, with architectures and configurations detailed in Appendices A.4 and A.12.

3.3 TOKENIZERS

This study employs eight tokenizers spanning character-level, atom-level, and motif-level methods. These include a simple character-level tokenizer (vocab size: 48), an atom-level Atom-in-SMILES (AIS) tokenizer (vocab size: 1023) designed to encode atomic environments (Ucak et al., 2023), and six byte-pair encoding (BPE) variants. One BPE tokenizer is adopted directly from DeepChem's Hugging Face model <code>seyonec/PubChem10M_SMILES_BPE_450k^5</code> with a vocabulary of 7,924 tokens, though only around 1,700 are used for 1M NPs. The remaining five BPE tokenizers (NPBPE) are trained on 1M NPs using Hugging Face's <code>BpeTrainer^6</code>, with vocabulary sizes of 60, 100, 1,000, 7,924, and 30k. All tokenizers (except DeepChem's) were implemented using a part of the prebuilt functionalities from Hugging Face's <code>PreTrainedTokenizer</code> with fixed vocabulary files built from the 1M NPs. Tokenizer implementation details are provided in Appendix A.6, with examples of tokenized SMILES strings, Jaccard similarity between tokenizer vocabularies, and token Zipfian distributions shown in Appendix Table 7 and Figures 14 and 15.

3.4 EXPERIMENTAL DESIGN

The study begins by pre-training 48 model variants (from Mamba, Mamba-2, and GPT with eight tokenizers using both random and scaffold splits) on the 1M NPs split into training (80%), validation (10%), and test (10%) sets. Scaffold split separates molecules with the same scaffolds or core chemical structures into the same set, helping to better evaluate models' ability to generalize to structurally novel compounds. The scaffold splitter used in this study is DeepChem's ScaffoldSplitter⁸ class, which is based on the Bemis-Murcko scaffold representation.

Pre-training hyperparameters are optimized via random search on 5% of the training/validation data. SMILES sequences are truncated or padded to a fixed length of 512 tokens and trained with cross-entropy loss using the optimized hyperparameters for each model/tokenizer pair until convergence (≤150 epochs with early stopping, patience = 5 epochs). Afterwards, they are evaluated on an unseen test set. The total training time for each model ranges from hours to a week. The parameter counts for each model range from 8.96M to 69.7M (see Appendix A.12 for details). All models are trained with Sharpness-Aware Minimization (SAM), adopting the implementation from Tsai et al. (2024). SAM is an optimization technique that encourages convergence to flatter loss minima, which are associated with better generalization performance (Foret et al., 2020).

Fine-tuning is conducted on three downstream tasks using the 48 pre-trained models and two additional models, MoLFormer and ChemBERTa-2 (Ross et al., 2022; Ahmad et al., 2022), which undergo a two-step fine-tuning process: with or without being fine-tuned on the 1M NPs first before being fine-tuned for downstream tasks. MoLFormer is an encoder-only transformer-based CLM that learns chemical representations from SMILES using rotary positional embeddings, linear attention, and Regex-based tokenization; in this study, we use the MoLFormer-XL-both-10pct variant, which has been pre-trained on a 10% subset (~100M) of PubChem and ZINC, and performs comparably to the full-scale MoLFormer-XL (Ross et al., 2022). ChemBERTa-2 is a RoBERTa-based transformer pre-trained on 77M SMILES from PubChem; in this study, we fine-tune the MLM vari-

 $^{^4} https://huggingface.co/docs/transformers/v4.51.3/en/model_doc/gpt2\#transformers.GPT2LMHeadModel$

⁵https://huggingface.co/seyonec/PubChem10M_SMILES_BPE_450k

 $^{^6}$ https://huggingface.co/docs/tokenizers/en/api/trainers#tokenizers.trainers.BpeTrainer

⁷https://huggingface.co/docs/transformers/v4.51.3/en/main_classes/tokenizer#transformers.PreTrainedTokenizer

 $^{^8 \}rm https://deepchem.readthedocs.io/en/latest/api_reference/splitters.html <math display="inline">\# scaffoldsplitter$

ant on 1M NPs, while using the more computationally intensive MTR variant directly for property prediction (Ahmad et al., 2022). Details can be found in Appendices A.4.3 and A.4.4.

Property prediction is performed by replacing each model's language modeling heads with classification heads. Each task is evaluated via repeated 5×5-fold cross-validation with hyperparameter tuning, early stopping, and results are averaged over runs with standard errors (SE) (Figures 16 and 17 in the Appendix). Loss function for the FourTastes dataset is CrossEntropyLoss() with class weighting since it is an imbalanced multi-class task, while BCEWithLogitsLoss() with-

				D	ownstre	am Task	s		
			Property Prediction						
	Pre-training*/ Fine-tuning** on 1M NP Data Split	Peptide Permeability (AUC-ROC ± SE)		FourTastes (MCC±SE)		Anti-Cancer Activities (MCC ± SE)		Molecule Generation (novel, valid, unique	
Models		scaffold	random	scaffold	random	scaffold	random	NP-Likess, SAScore)	
NP Pre-trained Models	scaffold*	✓	✓	✓	✓	✓	✓	✓	
(current study, 48 models)	random*	1	1	✓	1	1	✓	✓	
MolFormer	×	✓	✓	Х	Х	✓	✓		
(MoLFormer-XL-both-10pct)	random**	1	1	Х	Х	1	1		
ChemBERTa-2	×	✓	✓	Х	Х	✓	✓	n.a.	
(ChemBERTa-77M-MLM)	random**	1	1	Х	Х	1	1	11.3.	
ChemBERTa-2 (ChemBERTa-77M-MTR)	х	✓	✓	х	х	✓	✓		

Figure 2: Downstream application overview.

out weighting is applied to the more balanced anti-cancer and peptide permeability binary prediction tasks. Evaluation metrics include Area Under the Receiver Operating Characteristic Curve (AUC-ROC) and Matthews Correlation Coefficient (MCC). **Molecule generation** is performed via autoregressive sampling with a temperature of one and a maximum sequence length of 512 tokens. Each of the 48 pre-trained models generates 100k SMILES sequences, and they are assessed for validity (% of chemically valid SMILES strings, as determined by RDKit), uniqueness (% of non-duplicate valid molecules), and novelty (% of valid, unique molecules not found in 1M NPs). Figures 1 and 2 provide an overview of the experimental design and downstream task application. All pre-trained models, implementation code, and generated pseudo-NP SMILES in this work will be made publicly available via Hugging Face and GitHub upon acceptance.

4 RESULTS

4.1 MOLECULE GENERATION

Model and tokenizer choices give rise to three general trends. First, tokenizers with smaller or chemically informed vocabularies (e.g., Character-level, AIS, NPBPE60/100) outperform larger vocabulary ones in validity, uniqueness, and novelty by around 10-20%. Second, Mamba yields 1-2% higher validity and uniqueness, while GPT generates around 2% more novel molecules and scaffolds. Third, tokenizer choice significantly impacts performance.

Table 1: Tokenizer- and model-wise average percentages of valid, unique, and novel molecules: values for random and scaffold split pre-trained models and their average; "novel" refers to not being present in the 1M NP training data.

	R	Random Sp	lit	S	caffold Spl	it		Average		
	Valid	Unique	Novel	Valid	Unique	Novel	Valid	Unique	Novel	
Tokenizer-wise Avg.										
Character-level	80.68%	79.85%	70.23%	79.26%	78.17%	66.94%	79.97%	79.01%	68.58%	
AIS	81.43%	80.25%	70.41%	81.09%	79.73%	68.85%	81.26%	79.99%	69.63%	
BPE	78.09%	77.12%	66.66%	78.79%	77.55%	65.31%	78.44%	77.34%	65.99%	
NPBPE60	80.33%	79.34%	68.10%	79.05%	77.97%	68.03%	79.69%	78.65%	68.06%	
NPBPE100	80.60%	79.46%	67.85%	81.02%	79.45%	67.06%	80.81%	79.45%	67.46%	
NPBPE1000	80.81%	79.14%	64.30%	79.65%	77.36%	61.06%	80.23%	78.25%	62.68%	
NPBPE7924	68.50%	66.39%	53.18%	69.04%	66.25%	51.14%	68.77%	66.32%	52.16%	
NPBPE30k	57.29%	54.94%	45.24%	50.25%	47.43%	37.92%	53.77%	51.19%	41.58%	
Model-wise Avg.										
Mamba-2	74.70%	73.42%	61.80%	74.51%	72.69%	58.90%	74.60%	73.05%	60.35%	
Mamba	77.25%	75.91%	63.11%	75.28%	73.64%	61.35%	76.27%	74.77%	62.23%	
GPT	75.95%	74.36%	64.83%	74.52%	72.64%	62.11%	75.23%	73.50%	63.47%	

Tokenizer impact on generation performance shows that AIS achieves the highest molecule validity, uniqueness, and novelty, on average 1-2% higher than the character-level and small vocabulary NPBPE variants, which perform second best (see Table 1). In contrast, larger NPBPE tokenizers (e.g., NPBPE7924/30k) show substantially degraded performance, around 12-28% lower on average than AIS, potentially due to excessive vocabulary size. This aligns with the findings from Aksamit et al. (2024), which shows that overly large vocabularies lead to sparse token usage and hinder efficient chemical language modeling.

Table 2 shows that tokenizers with more fine-grained tokens, like character-level and NPBPE60, however, yielded more unique and novel scaffolds (Murcko scaffolds extracted from the generated molecules using RDKit's GetScaffoldForMol⁹), contrasting with the earlier observation that the AIS tokenizer is more effective for molecules. Scaffolds may benefit from finer-grained tokenization because they involve core substructures that recur with subtle variations, and fine-grained tokens offer such flexibility. Scaffold sets generated by the 48 models also show low pairwise Jaccard similarity values (from 0.05 to 0.11), suggesting that different models are exploring fairly distinct chemical spaces (Figure 23 in the Appendix). The scaffold distribution in the 1M NPs follows Zipf's law, and so do the scaffolds from the generated molecules (Figure 22 in the Appendix). Novel scaffolds predominantly appear in the long tail of the distribution, typically occurring fewer than 10 times each, reflecting their low frequency and high diversity.

Model Influence on molecule generation is more subtle compared to the influence of tokenizers. However, on average, Mamba still yields 1.4% higher validity and uniqueness than Mamba-2 and GPT. In contrast, GPT outperforms Mamba and Mamba-2 by approximately 2% on average in generating novel molecules and has generated about 1-2k more novel scaffolds (see Tables 1 and 2). Mamba's selective SSM (S6) architecture is less effective than transformers in forming entirely novel molecules, likely due to its

270

271

272

273

274

275

276

277

278

279

280

281

282

283

284

285

286

287

288

289

290

291

292

293

294

295

296

297

298

299

300

301

302

303 304

305

306

307

308

309

310

311

312

313

314

315

316

317

318

319

320

321

322

323

Table 2: **Tokenizer- and model-wise average unique and novel scaffold counts:** values for random and scaffold split pre-trained models and their average.

	Randor	n Split	Scaffol	d Split	Aver	age
	Unique	Novel	Unique	Novel	Unique	Novel
Tokenizer-wise Avg.						
Character-level	43641	33757	34000	25134	38821	29446
AIS	40014	29184	32306	22377	36160	25781
BPE	41372	31972	33750	24742	37561	28357
NPBPE60	42637	32001	36323	28406	39480	30204
NPBPE100	42825	32338	34793	25892	38809	29115
NPBPE1000	41385	29461	31183	21060	36284	25261
NPBPE7924	35500	25957	28172	19867	31836	22912
NPBPE30k	30183	23133	20971	15811	25577	19472
Model-wise Avg.						
Mamba-2	39313	29067	30315	21266	34814	25166
Mamba	40355	29394	31878	23016	36117	26205
GPT	39415	30716	32119	24452	35767	27584

local, sequential update and the hidden state decay in its global channels, as discovered by Ye et al. (2025), which together limit the holistic understanding required for novelty. In contrast, self-attention's attending to all tokens at each step likely enables more flexible token recombination than Mamba. Mamba outperforms Mamba-2 in producing more valid, unique, and novel molecules. This aligns with the expected trade-off in Mamba-2 between inference expressivity and hardware efficiency; namely, by replacing a diagonal with a scalar-times-identity structure in its SSM, Mamba-2 reduces expressivity, while Mamba retains more flexible, independently controlled channels (Gu & Dao, 2024; Dao & Gu, 2024; Dao, 2024).

Training and inference efficiency varies by model architecture and tokenizer. Larger-vocabulary NPBPE tokenizers reduce the average tokenized sequence length by approximately 3- to 6-fold (from around 70 tokens with a character-level tokenizer to 10-20 tokens) and often result in an average 2- to 4-fold increase in training speed, though at the cost of reduced generation quality. Additionally, NPBPE60 and 100 achieve performance nearly as well as Character-level and AIS tokenizers while halving sequence length through only a few simple merges (e.g., "C(", "CC", "O)", "[C", "[C@", "cc"), showing that optimized tokenization can reduces memory and compute while maintaining performance. Furthermore, hyperparameter search also consistently leads to Mamba and Mamba-2 models adopting deeper architectures (with more stacked Mamba blocks) than GPT models, leading to slower training and inference than GPT, which tends to select fewer transformer blocks (Figures 28, 29, and 30 in the Appendix). Specific model-tokenizer pairs, like M1+NPBPE100 and GPT+NPBPE100, balance outstanding overall performance and speed, with over 50% faster training and up to 12 times faster inference than the worst-performing ones. GPT+AIS and GPT+NPBPE60 are the most efficient and competitive for novel scaffolds. These results underscore the importance of aligning model-tokenizer choices with specific goals for optimal outcomes.

It is worth noting that while evaluating the synthesizability of machine-generated pseudo-NPs is important, it remains highly challenging. Although advances in AI-assisted synthesis planning (e.g., AiZynthFinder, Chemformer, RXN, Synthia, ASKCOS, ICSYNTH) show promise, these tools re-

⁹https://www.rdkit.org/docs/source/rdkit.Chem.Scaffolds.MurckoScaffold. html

main limited primarily to simpler or moderately complex molecules, with automated routes for highly intricate, sp³-rich NPs still unreliable and often requiring extensive expert intervention and validation (Gangwal & Lavecchia, 2025). For additional discussion and evaluation on synthetic accessibility, see Appendix A.11. Ultimately, the primary goal of this study is not practical synthesis, but to understand and evaluate how well models and tokenizers learn NP properties and explore their chemical space.

Error analysis is therefore conducted by using partialsmiles 2.0, a Python library that parses partial SMILES to detect syntax, valence, and kekulization errors (O'Boyle, 2020). Across all models, there is a clear pattern of syntax errors dominating around 80% of the molecules rejected by partialsmiles, and nearly half of them arising from unclosed rings (Table 3 and Appendix Table 9). While valence errors reflect local inconsistencies, and kekulization failures stem more from global graph-level constraints, certain syntax errors can provide insight into how well a model handles long-range dependency. As shown in Table 3, Mamba generates 6.15% and 3.73% fewer long-range syntax errors than GPT and Mamba-2, while also producing more valid and unique molecules (Table 1). Mamba is less effective at novelty compared to GPT; nevertheless, Mamba has produced much fewer long-range dependency related errors, and its selective SSM updates provide more structural stability in contrast with GPT's flexible but more error-prone novel token recombinations. Similar robustness has been noted previously, with S4 (the predecessor of Mamba) shown to capture long-distance dependencies and reduce SMILES design errors more reliably than GPT (Özçelik et al., 2024), and Mamba demonstrated to possess Lyapunov-stable recurrent dynamics that prevent divergence under perturbations (Halloran et al., 2025).

Table 3: Model- and tokenizer-wise average of syntax errors related to long-range dependency. All values are in % and are calculated by dividing the count of each error type by the total number of molecules rejected by the partialsmiles library.

Syntax Error Type	GPT	M1	M2	Char	BPE	AIS	60	100	1000	7924	30k
N ring openings have not been closed	48.32	47.58	44.76	42.74	46.72	48.38	44.85	45.72	48.70	51.42	46.60
Unmatched close parenthesis	14.82	13.20	18.18	17.11	11.75	15.57	13.90	12.59	11.26	16.87	24.18
N branches have not been closed	8.62	4.30	5.84	5.33	7.62	7.41	7.78	5.56	4.13	5.57	6.63
Missing the close bracket	0.66	0.92	0.97	1.81	2.23	0.00	1.38	0.86	0.43	0.06	0.03
The final branch should not be within parentheses	0.39	0.65	0.62	0.39	0.19	0.14	0.38	0.57	0.69	0.87	1.19
An open square bracket without close bracket	0.01	0.02	0.03	0.06	0.01	0.00	0.03	0.02	0.02	0.00	0.00
Total	72.82	66.67	70.40	67.44	68.52	71.50	68.32	65.32	65.23	74.79	78.63

M1 = Mamba, M2 = Mamba-2; numeric labels (60, 100, 1000, 7924, 30k) refer to NPBPE variants with corresponding vocabulary sizes.

4.2 Property Prediction

This section introduces the evaluation of 48 NP pre-trained models alongside MoLFormer and ChemBERTa-2 across three downstream property prediction tasks: molecular taste, anti-cancer activity, and peptide membrane permeability prediction. The analysis examines how tokenizer choice, model architecture, fine-tuning, and data splitting influence performance across these tasks.

Tokenizer choice has a substantial impact on model performance in downstream tasks, as shown by prior studies across natural, chemical, and protein language modeling (Dotan et al., 2024; Leon et al., 2024; Lindsey et al., 2024; Schmidt et al., 2024; Dagan et al., 2024; Suyunu et al., 2024; Tan et al., 2024). Same as for molecule generation, chemically informed tokenizers such as AIS and small, domain-adapted NPBPE variants (e.g., NPBPE60/100/1000) generally outperform larger vocabulary tokenizers like NPBPE7924 and NPBPE30k, as shown in Figures 3a and 3b. Peptide permeability prediction, however, shows less sensitivity to tokenizer and model variation, particularly under scaffold-split conditions (Figure 3c). This is likely because cyclic peptides have more uniform and constrained structures (Kurita & Numata, 2024). As a result, this task exhibits less variance, making it easier and less sensitive to model and tokenizer choices.

Impact of data splitting and model selection is evident from the clear performance drop observed when downstream task data are scaffold split (columns on the right in Figures 3 and 4), which challenges models to generalize by removing structural overlaps between training and test sets. In contrast, performance differences between scaffold and random splits on 1M NPs during pretraining are minimal. Model-wise, conditions of random splitting downstream data tend to highlight

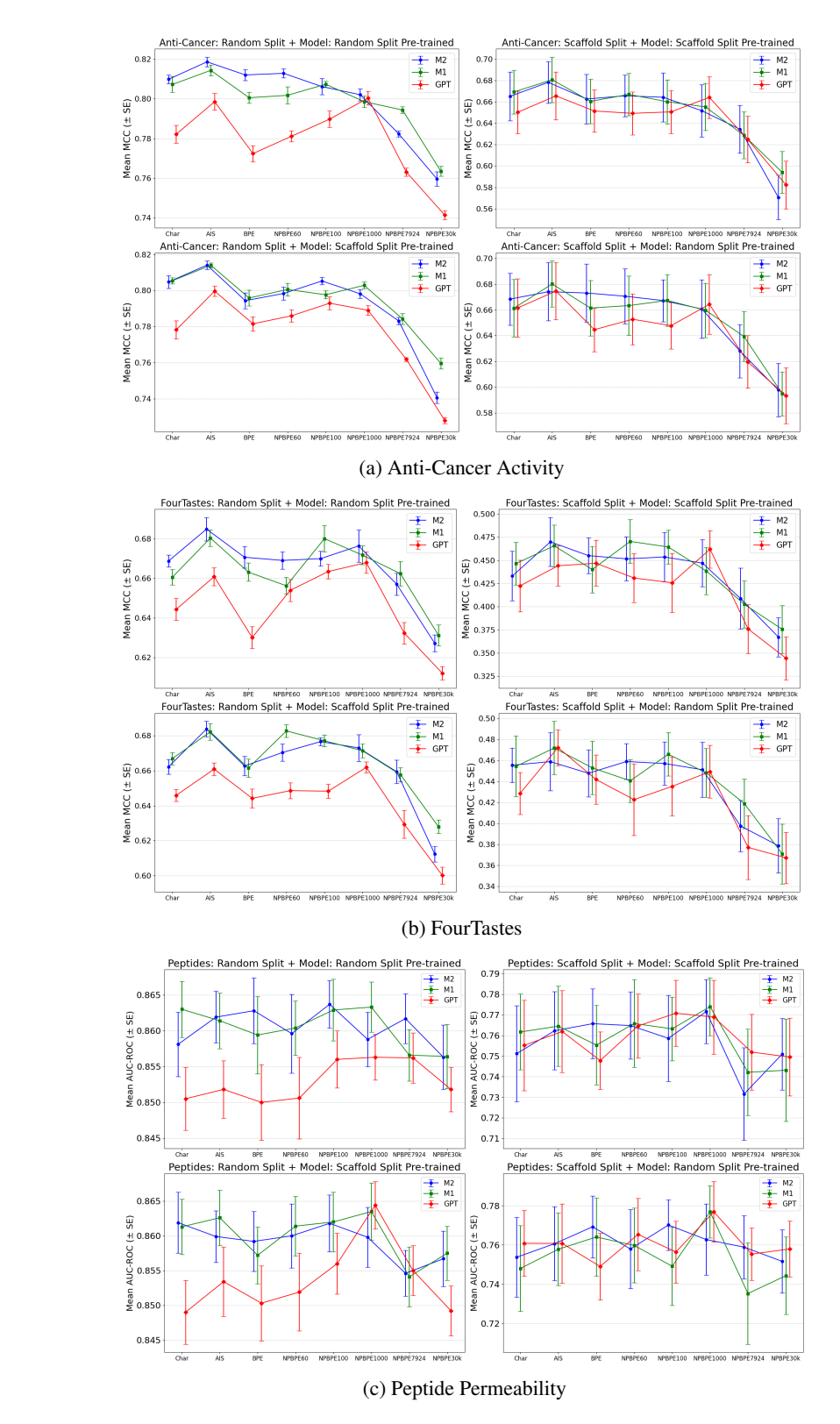


Figure 3: **Model performance comparison**: mean MCC and AUC-ROC (± SE) values across tokenizer and model pairs for three property prediction tasks with random and scaffold data split combinations.

433

434

435

436

437

438

439

440

441

442

443

444

445

446

447

448

449

450

451

452

453

454

455

456

457

458

459

460

461

462

463

464

465

466

467

468 469 470

471

472

473

474

475

476

477

478

479

480

481

482

483

484

485

architecture-related differences (columns on the left in Figures 3 and 4). Under random split, both Mamba models generally outperform GPT. A reason might be that Mamba's S6 dynamically prioritizes relevant information within a single sequence processing step to effectively capture local sequential dependencies (Gu & Dao, 2024). Mamba models can use such learned patterns readily and directly under random split conditions, where training and test sets share similar molecular scaffolds. For tasks that require more local focus, such a way of learning local patterns may be more effective than self-attention, which attends to all tokens at every step. Recurrent models have also been reported to provide better learning of local patterns than self-attention, which is better at capturing more global properties (Chen et al., 2023). Since Mamba is built upon SSMs, which are inherently recurrent, it might have also inherited this behavioral feature. Scaffold splitting downstream task data, however, requires models to capture more abstract, global chemical properties that extend beyond local motifs—a scenario in which neither Mamba's local focus nor GPT's inherently global self-attention seems to provide a clear advantage.

Pre-training vs. fine-tuning on NPs shows that NP-specific models trained on just 1M NP molecules can match the performance of CLMs (ChemBERTa-2 and MoLFormer) with large-scale pre-training data (77–110 times larger). In the anticancer activity task (Figure 4a), the Mamba model with AIS tokenizer performs nearly on par with MoL-Former under random split. Although MoLFormer (without NP fine-tuning) performs best, the gains are marginal and may not justify the much larger pre-training dataset. For peptide per-

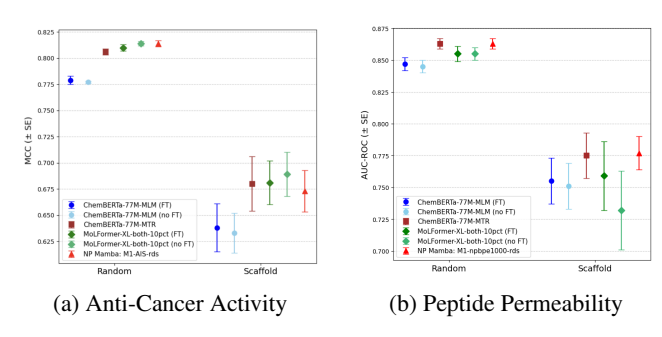


Figure 4: **Model performance comparison**: mean MCC and AUC-ROC (± SE) values for all models with and without fine-tuning (FT) on 1M NPs.

meability (Figure 4b), the NP Mamba model performed almost the same as ChemBERTa-77M-MTR under both random and scaffold split. Additionally, fine-tuning MoLFormer and ChemBERTa-77M-MLM on 1M NPs yields minor improvements. These observations have demonstrated the value of domain-specific pre-training, and they align with findings from other studies, which demonstrate that broad pre-training may introduce noisy or irrelevant features for the usually more specialized tasks in fields such as cheminformatics, bioinformatics, and material science (Kirschbaum & Bande, 2024; Skinnider et al., 2021; Fournier et al., 2024; Ghunaim et al., 2025; Li et al., 2023b). While training domain-specific CLMs from scratch offers greater control over data quality and avoids reproducibility issues, it demands substantial computational resources. Alternatively, Sultan et al. (2025) report that partial pre-training on relevant data (reduced-scale pre-training plus domain adaptation) can yield better performance, highlighting a trade-off between flexibility and efficiency.

5 Conclusion

This work addresses the underrepresentation of NPs in chemical language modeling by developing NPCLMs using both selective SSMs (Mamba, Mamba-2) and transformer (GPT) architectures. Through a systematic comparison across eight tokenization strategies and two downstream tasks (molecule generation and property prediction), we demonstrate that Mamba generates more valid and unique molecules while making fewer long-range dependency errors. However, GPT excels in novelty. Mamba and Mamba-2 also slightly outperform GPT in property prediction under random splits, though performance aligns under scaffold splits. The tokenization strategy strongly influences the results: chemically informed and domain-specific tokenizers with appropriate token frequency distribution outperform others. Domain-specific pre-training proves to be effective and can match the performance of fine-tuned general CLMs, emphasizing the importance of data relevance and quality over volume. In essence, for information-dense sequences, selective SSMs tend to preserve structural validity and long-range consistency, whereas self-attention favors recombination and novelty. Future work should examine whether these insights extend beyond the domain of NPs, while also aiming to advance tools to assess the synthesizability of machine-generated NP molecules, explore alternative inference and training methods, and investigate model size, architecture, and training data volume trade-offs.

REPRODUCIBILITY STATEMENT

We have taken comprehensive steps to ensure the reproducibility of our work. (1) Datasets: The pre-training and downstream property prediction datasets, together with all preprocessing steps, are described in Section 3.1 of the main text and detailed in Appendix A.3. We have included the random split version of the 1M NP dataset and the first-fold random split of the three downstream tasks in the supplementary material's data folder. (2) Tokenizers: Implementations of all tokenizers and their vocabulary files are provided in the tokenisers.py file and the vocab_files directory in the supplementary repository. (3) Experimental setup: The design of training, hyperparameter search, and fine-tuning procedures for all models is documented in Section 3.4 of the main text, with full details in Appendices A.7 and A.12. (4) Code and scripts: The supplementary repository includes a Dockerfile to build the training environment and a main.py entry point for running all tasks. A run_experiments.sh script is provided as a template to execute pre-training, fine-tuning, hyperparameter search, and molecule generation with minimal configuration; users can uncomment the relevant blocks to reproduce specific experiments. One pretrained model (M1-npbpe60-rds) is provided for demonstration. Upon acceptance, all 48 pretrained models, dataset splits, and generated molecules will be released on Hugging Face and GitHub. (5) Execution instructions: The supplementary repository's README file contains step-by-step instructions to rerun all major experiments reported in the paper, ensuring that results can be reproduced end-to-end without ambiguity.

REFERENCES

- Walid Ahmad, Elana Simon, Seyone Chithrananda, Gabriel Grand, and Bharath Ramsundar. Chemberta-2: Towards chemical foundation models. *arXiv:2209.01712*, 2022. URL https://arxiv.org/abs/2209.01712.
- Nicholas Aksamit, Alain Tchagang, Yifeng Li, and Beatrice Ombuki-Berman. Hybrid fragment-smiles tokenization for admet prediction in drug discovery. *BMC Bioinformatics*, 25(1):255, August 2024. ISSN 1471-2105. doi: 10.1186/s12859-024-05861-z. URL https://doi.org/10.1186/s12859-024-05861-z.
- R. Al-Jarf, A. G. C. de Sá, D. E. V. Pires, and D. B. Ascher. pdcsm-cancer: Using graph-based signatures to identify small molecules with anticancer properties. *Journal of Chemical Information and Modeling*, 61(7):3314–3322, 2021. doi: 10.1021/acs.jcim.1c00168.
- Lampros Androutsos, Lorenzo Pallante, Agorakis Bompotas, Filip Stojceski, Gianvito Grasso, Dario Piga, Giacomo Di Benedetto, Christos Alexakos, Athanasios Kalogeras, Konstantinos Theofilatos, Marco A. Deriu, and Seferina Mavroudi. Predicting multiple taste sensations with a multiobjective machine learning method. *npj Science of Food*, 8(1):47, July 2024. ISSN 2396-8370. doi: 10.1038/s41538-024-00287-6. URL https://doi.org/10.1038/s41538-024-00287-6.
- Juergen Bajorath. Chemical language models for molecular design. *Molecular Informatics*, 43, 2023. URL https://api.semanticscholar.org/CorpusID:265462871.
- Guy W Bemis and Mark A Murcko. The properties of known drugs. 1. molecular frameworks. *Journal of Medicinal Chemistry*, 39(15):2887–2893, Jul 1996. doi: 10.1021/jm9602928.
- Andres M. Bran and Philippe Schwaller. *Transformers and Large Language Models for Chemistry and Drug Discovery*, pp. 143–163. Springer Nature Singapore, Singapore, 2024. ISBN 978-981-97-4828-0. doi: 10.1007/978-981-97-4828-0.8. URL https://doi.org/10.1007/978-981-97-4828-0_8.
- Emilio Vital Brazil, Eduardo Soares, Victor Yukio Shirasuna, Renato Cerqueira, Dmitry Zubarev, and Kristin Schmidt. A mamba-based foundation model for chemistry. In *Neurips 2024 Workshop Foundation Models for Science: Progress, Opportunities, and Challenges*, 2024. URL https://openreview.net/forum?id=g0B9DtkDVk.
- Y. Chen, Z. Wang, X. Zeng, Y. Li, P. Li, X. Ye, and T. Sakurai. Molecular language models: Rnns or transformer? *Brief Funct Genomics*, 22(4):392–400, jul 2023. doi: 10.1093/bfgp/elad012.

- Ya Chen, Cara Rosenkranz, Steffen Hirte, and Johannes Kirchmair. Ring systems in natural products: structural diversity, physicochemical properties, and coverage by synthetic compounds. *Natural Product Reports*, 39(8):1544–1556, Aug 17 2022. ISSN 1460-4752. doi: 10.1039/d2np00001f. URL https://doi.org/10.1039/d2np00001f.
 - Gautier Dagan, Gabriel Synnaeve, and Baptiste Rozière. Getting the most out of your tokenizer for pre-training and domain adaptation. In *Proceedings of the 41st International Conference on Machine Learning*, ICML'24. JMLR.org, 2024.
 - Tri Dao. State Space Duality (Mamba-2) Part I IV. https://tridao.me/blog/, 2024. Accessed: 2024-10-07.
 - Tri Dao and Albert Gu. Transformers are SSMs: Generalized models and efficient algorithms through structured state space duality. *arXiv:2405.21060v1*, 2024. URL https://arxiv.org/abs/2405.21060.
 - Daniel A. Dias, Sylvia Urban, and Ute Roessner. A historical overview of natural products in drug discovery. *Metabolites*, 2(2):303–336, Apr 2012. doi: 10.3390/metabo2020303. URL https://www.mdpi.com/2218-1989/2/2/303.
 - Edo Dotan, Gal Jaschek, Tal Pupko, and Yonatan Belinkov. Effect of tokenization on transformers for biological sequences. *Bioinformatics*, 40(4):btae196, 04 2024. ISSN 1367-4811. doi: 10. 1093/bioinformatics/btae196. URL https://doi.org/10.1093/bioinformatics/btae196.
 - Peter Ertl and Ansgar Schuffenhauer. *Cheminformatics analysis of natural products: Lessons from nature inspiring the design of new drugs. In: Natural Compounds as Drugs: Volume II*, pp. 217–235. Birkhäuser Basel, Basel, 2008. doi: 10.1007/978-3-7643-8595-8_4. URL https://doi.org/10.1007/978-3-7643-8595-8_4.
 - Peter Ertl and Ansgar Schuffenhauer. Estimation of synthetic accessibility score of drug-like molecules based on molecular complexity and fragment contributions. *Journal of Cheminformatics*, 1(1):8, 2009. ISSN 1758-2946. doi: 10.1186/1758-2946-1-8. URL https://doi.org/10.1186/1758-2946-1-8.
 - Peter Ertl, Silvio Roggo, and Ansgar Schuffenhauer. Natural product-likeness score and its application for prioritization of compound libraries. *Journal of Chemical Information and Modeling*, 48(1):68–74, 2008. doi: 10.1021/ci700286x. URL https://doi.org/10.1021/ci700286x. PMID: 18034468.
 - Aaron L. Feller and Claus O. Wilke. Peptide-aware chemical language model successfully predicts membrane diffusion of cyclic peptides. *Journal of Chemical Information and Modeling*, 65(2): 571–579, 2025. doi: 10.1021/acs.jcim.4c01441. URL https://doi.org/10.1021/acs.jcim.4c01441. PMID: 39772542.
 - Richard Firn. *Nature's Chemicals: The Natural Products that shaped our world.* Oxford University Press, 11 2009. ISBN 9780199566839. doi: 10.1093/acprof:oso/9780199566839.001.0001. URL https://doi.org/10.1093/acprof:oso/9780199566839.001.0001.
 - Pierre Foret, Ariel Kleiner, Hossein Mobahi, and Behnam Neyshabur. Sharpness-aware minimization for efficiently improving generalization. *ArXiv*, abs/2010.01412, 2020. URL https://api.semanticscholar.org/CorpusID:222134093.
 - Quentin Fournier, Robert M. Vernon, Almer van der Sloot, Benjamin Schulz, Sarath Chandar, and Christopher James Langmead. Protein language models: Is scaling necessary? bioRxiv:https://doi.org/10.1101/2024.09.23.614603, 2024. URL https://api.semanticscholar.org/CorpusID:272884725.
 - Kathleen Gallo, Emanuel Kemmler, Andrean Goede, Finnja Becker, Mathias Dunkel, Robert Preissner, and Priyanka Banerjee. SuperNatural 3.0—a database of natural products and natural product-based derivatives. *Nucleic Acids Research*, 51(D1):D654–D659, 11 2022. ISSN 0305-1048. doi: 10.1093/nar/gkac1008. URL https://doi.org/10.1093/nar/gkac1008.

- Amit Gangwal and Antonio Lavecchia. Artificial intelligence in natural product drug discovery:
 Current applications and future perspectives. *Journal of Medicinal Chemistry*, 68(4):3948–3969,
 2025. ISSN 0022-2623. doi: 10.1021/acs.jmedchem.4c01257. URL https://doi.org/10.
 1021/acs.jmedchem.4c01257.
 - Wenhao Gao and Connor W. Coley. The synthesizability of molecules proposed by generative models. *Journal of Chemical Information and Modeling*, 60(12):5714-5723, 2020. doi: 10.1021/acs.jcim.0c00174. URL https://doi.org/10.1021/acs.jcim.0c00174. PMID: 32250616.
 - Yasir Ghunaim, Hasan Abed Al Kader Hammoud, and Bernard Ghanem. Towards data-efficient pretraining for atomic property prediction. *arXiv:2502.11085*, 2025. URL https://arxiv.org/abs/2502.11085.
 - Jeffrey W. Godden and Jürgen Bajorath. Differential shannon entropy as a sensitive measure of differences in database variability of molecular descriptors. *Journal of Chemical Information and Computer Sciences*, 41(4):1060–1066, 2001. doi: 10.1021/ci0102867. URL https://doi.org/10.1021/ci0102867. PMID: 11500125.
 - Albert Gu and Tri Dao. Mamba: Linear-time sequence modeling with selective state spaces. *arXiv:2312.00752v2*, 2024. URL https://arxiv.org/abs/2312.00752.
 - John Timothy Halloran, Manbir S Gulati, and Paul F Roysdon. Mamba state-space models are lyapunov-stable learners. In *ICLR 2025 Workshop on Deep Generative Model in Machine Learning: Theory, Principle and Efficacy*, 2025. URL https://openreview.net/forum?id=XDfyJqlB4T.
 - A. Harvey, R. Edrada-Ebel, and R. Quinn. The re-emergence of natural products for drug discovery in the genomics era. *Nature Reviews Drug Discovery*, 14:111–129, 2015. doi: 10.1038/nrd4510.
 - Ye Hu, Dagmar Stumpfe, and J. Bajorath. Lessons learned from molecular scaffold analysis. *Journal of chemical information and modeling*, 51 8:1742–53, 2011. doi: 10.1021/ci200179y.
 - Ye Hu, Dagmar Stumpfe, and J. Bajorath. Computational exploration of molecular scaffolds in medicinal chemistry. *Journal of medicinal chemistry*, 59 9:4062–76, 2016. doi: 10.1021/acs.jmedchem.5b01746.
 - Kevin Maik Jablonka, Philippe Schwaller, Andres Ortega-Guerrero, and Berend Smit. Leveraging large language models for predictive chemistry. *Nat. Mac. Intell.*, 6:161–169, 2024. URL https://api.semanticscholar.org/CorpusID:267538205.
 - Jared Kaplan, Sam McCandlish, Tom Henighan, Tom B. Brown, Benjamin Chess, Rewon Child, Scott Gray, Alec Radford, Jeffrey Wu, and Dario Amodei. Scaling laws for neural language models. arXiv:2001.08361, 2020. URL https://arxiv.org/abs/2001.08361.
 - Thorren Kirschbaum and Annika Bande. Transfer learning for molecular property predictions from small data sets. *arXiv:2404.13393*, 2024. URL https://arxiv.org/abs/2404.13393.
 - Taichi Kurita and Keiji Numata. The structural and functional impacts of rationally designed cyclic peptides on self-assembly-mediated functionality. *Phys. Chem. Chem. Phys.*, 26:28776–28792, 2024. doi: 10.1039/D4CP02759K. URL http://dx.doi.org/10.1039/D4CP02759K.
 - Miguelangel Leon, Yuriy Perezhohin, Fernando Peres, Aleš Popovič, and Mauro Castelli. Comparing smiles and selfies tokenization for enhanced chemical language modeling. *Scientific Reports*, 14(1):25016, October 2024. ISSN 2045-2322. doi: 10.1038/s41598-024-76440-8. URL https://doi.org/10.1038/s41598-024-76440-8.
 - Gong-Hua Li and Jing-Fei Huang. Cdrug: a web server for predicting anticancer activity of chemical compounds. *Bioinformatics*, 28(24):3334–3335, 2012. ISSN 1367-4803. doi: 10.1093/bioinformatics/bts625. URL https://doi.org/10.1093/bioinformatics/bts625.

- Jianan Li, Keisuke Yanagisawa, Masatake Sugita, Takuya Fujie, Masahito Ohue, and Yutaka Akiyama. Cycpeptmpdb: A comprehensive database of membrane permeability of cyclic peptides. *Journal of Chemical Information and Modeling*, 63(7):2240–2250, 2023a. doi: 10.1021/acs.jcim.2c01573. URL https://doi.org/10.1021/acs.jcim.2c01573.
 - K. Li, D. Persaud, K. Choudhary, B. DeCost, M. Greenwood, and J. Hattrick-Simpers. Exploiting redundancy in large materials datasets for efficient machine learning with less data. *Nature Communications*, 14(1):7283, 2023b. doi: 10.1038/s41467-023-42992-y.
 - Xinhao Li and Denis Fourches. Smiles pair encoding: A data-driven substructure tokenization algorithm for deep learning. *Journal of chemical information and modeling*, 2020. URL https://api.semanticscholar.org/CorpusID:220423591.
 - Chang Liao, Yemin Yu, Yu Mei, and Ying Wei. From words to molecules: A survey of large language models in chemistry. *arXiv:2402.01439v1*, 2024. URL https://api.semanticscholar.org/CorpusID:267406767.
 - LeAnn M. Lindsey, Nicole L. Pershing, Anisa Habib, W. Zac Stephens, Anne J. Blaschke, and Hari Sundar. A comparison of tokenization impact in attention based and state space genomic language models. *BioRxiv*, 2024. doi: 10.1101/2024.09.09.612081. URL https://doi.org/10.1101/2024.09.09.612081. bioRxiv preprint, not peer-reviewed.
 - Jieyu Lu and Yingkai Zhang. Unified deep learning model for multitask reaction predictions with explanation. *Journal of Chemical Information and Modeling*, 62(6):1376–1387, 2022. doi: 10. 1021/acs.jcim.1c01467. URL https://yzhang.hpc.nyu.edu/T5Chem. Epub 2022 Mar 10.
 - D. Newman and G. Cragg. Natural products as sources of new drugs from 1981 to 2014. *Journal of natural products*, 79 3:629–61, 2016. doi: 10.1021/acs.jnatprod.5b01055.
 - N. M. O'Boyle. partialsmiles, version 2.0. https://baoilleach.github.io/partialsmiles/index.html, 2020. Available from https://github.com/baoilleach/partialsmiles.
 - Zhangzhi Peng, Benjamin Schussheim, and Pranam Chatterjee. PTM-mamba: A ptm-aware protein language model with bidirectional gated mamba blocks. bioRxiv:10.1101/2024.02.28.581983, 2024. doi: 10.1101/2024.02.28.581983. URL https://www.biorxiv.org/content/early/2024/02/29/2024.02.28.581983.
 - C. Pye, M. Bertin, R. Lokey, W. Gerwick, and Roger G. Linington. Retrospective analysis of natural products provides insights for future discovery trends. *Proceedings of the National Academy of Sciences*, 114:5601 5606, 2017. doi: 10.1073/pnas.1614680114.
 - Jerret Ross, Brian Belgodere, Vijil Chenthamarakshan, Inkit Padhi, Youssef Mroueh, and Payel Das. Large-scale chemical language representations capture molecular structure and properties. *Nature Machine Intelligence*, 4(12):1256–1264, 2022. doi: 10.1038/s42256-022-00580-7.
 - Adriano Rutz, Maria Sorokina, Jakub Galgonek, Daniel Mietchen, Egon Willighagen, Arnaud Gaudry, James G. Graham, Ralf Stephan, Roderic Page, Jiří Vondrášek, Christoph Steinbeck, Guido F. Pauli, Jean-Luc Wolfender, Jonathan Bisson, and Pierre-Marie Allard. The lotus initiative for open knowledge management in natural products research. *eLife*, 11:e70780, 2022. doi: 10.7554/eLife.70780.
 - Koh Sakano, Kairi Furui, and Masahito Ohue. Npgpt: natural product-like compound generation with gpt-based chemical language models. *The Journal of Supercomputing*, 81(1):352, 2024. ISSN 1573-0484. doi: 10.1007/s11227-024-06860-w. URL https://doi.org/10.1007/s11227-024-06860-w.
 - F. I. Saldívar-González, V. D. Aldas-Bulos, J. L. Medina-Franco, and F. Plisson. Natural product drug discovery in the artificial intelligence era. *Chem. Sci.*, 13:1526–1546, 2022. doi: 10.1039/D1SC04471K. URL http://dx.doi.org/10.1039/D1SC04471K.
 - Daisuke Sato, Zhiyuan Wu, Hikaru Fujita, and J. Lindsey. Design, synthesis, and utility of defined molecular scaffolds. *Organics*, 2021. doi: 10.3390/ORG2030013.

- Craig W Schmidt, Varshini Reddy, Haoran Zhang, Alec Alameddine, Omri Uzan, Yuval Pinter, and Chris Tanner. Tokenization is more than compression. In Yaser Al-Onaizan, Mohit Bansal, and Yun-Nung Chen (eds.), *Proceedings of the 2024 Conference on Empirical Methods in Natural Language Processing*, pp. 678–702, Miami, Florida, USA, November 2024. Association for Computational Linguistics. doi: 10.18653/v1/2024.emnlp-main.40. URL https://aclanthology.org/2024.emnlp-main.40/.
 - Damiano Sgarbossa, Cyril Malbranke, and Anne-Florence Bitbol. ProtMamba: a homology-aware but alignment-free protein state space model. bioRxiv:10.1101/2024.05.24.595730, 2024. doi: 10. 1101/2024.05.24.595730. URL https://www.biorxiv.org/content/early/2024/05/25/2024.05.24.595730.
 - Xiaojuan Shen, Tao Zeng, Nianhang Chen, Jiabo Li, and Ruibo Wu. Nimo: A natural product-inspired molecular generative model based on conditional transformer. *Molecules*, 29(8), 2024. ISSN 1420-3049. doi: 10.3390/molecules29081867. URL https://www.mdpi.com/1420-3049/29/8/1867.
 - Michael A. Skinnider, R. Greg Stacey, David Scott Wishart, and Leonard J. Foster. Chemical language models enable navigation in sparsely populated chemical space. *Nature Machine Intelligence*, 3:759 770, 2021. URL https://api.semanticscholar.org/CorpusID: 237648365.
 - Maria Sorokina, Peter Merseburger, Kohulan Rajan, Mehmet Aziz Yirik, and Christoph Steinbeck. Coconut online: Collection of open natural products database. *Journal of Cheminformatics*, 13 (1):2, 2021. ISSN 1758-2946. doi: 10.1186/s13321-020-00478-9. URL https://doi.org/10.1186/s13321-020-00478-9.
 - Florence L. Stahura, Jeffrey W. Godden, Ling Xue, and Jürgen Bajorath. Distinguishing between natural products and synthetic molecules by descriptor shannon entropy analysis and binary qsar calculations. *Journal of Chemical Information and Computer Sciences*, 40(5):1245–1252, 2000. ISSN 0095-2338. doi: 10.1021/ci0003303. URL https://doi.org/10.1021/ci0003303.
 - Charles F. Stratton, David J. Newman, and Derek S. Tan. Cheminformatic comparison of approved drugs from natural product versus synthetic origins. *Bioorganic & Medicinal Chemistry Letters*, 25(21):4802–4807, 2015. doi: 10.1016/j.bmcl.2015.07.014.
 - Afnan Sultan, Jochen Sieg, Miriam Mathea, and Andrea Volkamer. Transformers for molecular property prediction: Lessons learned from the past five years. *Journal of Chemical Information and Modeling*, 64(16):6259–6280, 2024. doi: 10.1021/acs.jcim.4c00747. URL https://doi.org/10.1021/acs.jcim.4c00747.
 - Afnan Sultan, Max Rausch-Dupont, Shahrukh Khan, Olga Kalinina, Andrea Volkamer, and Dietrich Klakow. Transformers for molecular property prediction: Domain adaptation efficiently improves performance. *ArXiv*, abs/2503.03360, 2025. URL https://api.semanticscholar.org/CorpusID:276781915.
 - Burak Suyunu, Enes Taylan, and Arzucan Ozgur. Linguistic Laws Meet Protein Sequences: A Comparative Analysis of Subword Tokenization Methods. In 2024 IEEE International Conference on Bioinformatics and Biomedicine (BIBM), pp. 4489–4496, Los Alamitos, CA, USA, December 2024. IEEE Computer Society. doi: 10.1109/BIBM62325.2024.10822826. URL https://doi.ieeecomputersociety.org/10.1109/BIBM62325.2024.10822826.
 - Y. Tan, M. Li, Z. Zhou, P. Tan, H. Yu, G. Fan, and L. Hong. PETA: evaluating the impact of protein transfer learning with sub-word tokenization on downstream applications. *Journal of Cheminformatics*, 16(1):92, 2024. doi: 10.1186/s13321-024-00884-3.
- Dillon W. P. Tay, Naythan Z. X. Yeo, Krishnan Adaikkappan, Yee Hwee Lim, and Shi Jun Ang. 67 million natural product-like compound database generated via molecular language processing. *Scientific Data*, 10(1):296, 2023. ISSN 2052-4463. doi: 10.1038/s41597-023-02207-x. URL https://doi.org/10.1038/s41597-023-02207-x.

- Yi Tay, Mostafa Dehghani, Dara Bahri, and Donald Metzler. Efficient transformers: A survey. *ACM Comput. Surv.*, 55(6), Dec 2022. ISSN 0360-0300. doi: 10.1145/3530811. URL https://doi.org/10.1145/3530811.
- Vishrut Thoutam and Dina Ellsworth. MSAMamba: Adapting subquadratic models to long-context DNA MSA analysis. In *ICML* 2024 Workshop on Theoretical Foundations of Foundation Models, 2024. URL https://openreview.net/forum?id=PogdVDgGFT.
- Ting Yu Tsai, Li Lin, Shu Hu, Ming-Ching Chang, Hongtu Zhu, and Xin Wang. Uu-mamba: Uncertainty-aware u-mamba for cardiac image segmentation. *arXiv:2405.17496*, 2024.
- Zhengkai Tu, Sourabh J. Choure, Mun Hong Fong, Jihye Roh, Itai Levin, Kevin Yu, Joonyoung F. Joung, Nathan Morgan, Shih-Cheng Li, Xiaoqi Sun, Huiqian Lin, Mark Murnin, Jordan P. Liles, Thomas J. Struble, Michael E. Fortunato, Mengjie Liu, William H. Green, Klavs F. Jensen, and Connor W. Coley. Askcos: Open-source, data-driven synthesis planning. *Accounts of Chemical Research*, 58(11):1764–1775, 2025. ISSN 0001-4842. doi: 10.1021/acs.accounts.5c00155. URL https://doi.org/10.1021/acs.accounts.5c00155.
- Umit V. Ucak, Islambek Ashyrmamatov, and Juyong Lee. Improving the quality of chemical language model outcomes with atom-in-smiles tokenization. *Journal of Cheminformatics*, 15(1):55, 2023. ISSN 1758-2946. doi: 10.1186/s13321-023-00725-9. URL https://doi.org/10.1186/s13321-023-00725-9.
- Ashish Vaswani, Noam Shazeer, Niki Parmar, Jakob Uszkoreit, Llion Jones, Aidan N. Gomez, Łukasz Kaiser, and Illia Polosukhin. Attention is all you need. In *Proceedings of the 31st International Conference on Neural Information Processing Systems*, NIPS'17, pp. 6000–6010, Red Hook, NY, USA, 2017. Curran Associates Inc. ISBN 9781510860964.
- David Weininger. Smiles, a chemical language and information system. 1. introduction to methodology and encoding rules. *J. Chem. Inf. Comput. Sci.*, 28:31–36, 1988. URL https://api.semanticscholar.org/CorpusID:5445756.
- Bohao Xu, Yingzhou Lu, Chenhao Li, Ling Yue, Xiao Wang, Nan Hao, Tianfan Fu, and Jim Chen. Smiles-mamba: Chemical mamba foundation models for drug admet prediction. arXiv:2408.05696, 2024. URL https://arxiv.org/abs/2408.05696.
- Zhifan Ye, Kejing Xia, Yonggan Fu, Xin Dong, Jihoon Hong, Xiangchi Yuan, Shizhe Diao, Jan Kautz, Pavlo Molchanov, and Yingyan Celine Lin. Longmamba: Enhancing mamba's long-context capabilities via training-free receptive field enlargement. In *The Thirteenth International Conference on Learning Representations*, 2025. URL https://openreview.net/forum?id=fMbLszVO1H.
- Riza Ozçelik, Sarah de Ruiter, Emanuele Criscuolo, and Francesca Grisoni. Chemical language modeling with structured state space sequence models. *Nature Communications*, 15(1):6176, Jul 22 2024. ISSN 2041-1723. doi: 10.1038/s41467-024-50469-9. URL https://doi.org/10.1038/s41467-024-50469-9.

A	A	PPENDIX
Co	ONTE	ENTS
1	Intro	oduction
2	Rela	ted Work
3	Met	hodology
	3.1	Data
	3.2	Model
	3.3	Tokenizers
	3.4	Experimental Design
4	Resu	ılts
	4.1	Molecule Generation
	4.2	Property Prediction
5	Con	clusion
A		endix
		LLM Usage Disclosure
	A.2	Limitations
	A.3	Data
		A.3.1 Pre-training Data
		A.3.2 NP Downstream Dataset Availability and Task Selection
		A.3.3 Peptide Permeability
		A.3.4 FourTastes
		A.3.5 Anti-Cancer Activity
	A.4	Models
		A.4.1 GPT
		A.4.2 Mamba and Mamba-2
		A.4.3 MoLFormer
		A.4.4 ChemBERTa-2
	A.5	Related Work (Extended)
	A.6	Tokenization
		A.6.1 Character-level Tokenizer
		A.6.2 DeepChem Byte-Pair Encoding (BPE) Tokenizer
		A.6.3 Atom-In-SMILES (AIS) Tokenizer
		A.6.4 Natural Product Byte-Pair Encoding (NPBPE) Tokenizer
		A 6.5 When takenization fails

A.7	Fine-tuning on Downstream Tasks	30
	Molecule Generation Details	
A.9	Pseudo-NP Error Analysis	35
A.10	Scaffolds	37
A.11	Synthetic Accessibility & NP-Likeness	42
A.12	Pre-training Details	44

A.1 LLM USAGE DISCLOSURE

We have used ChatGPT (versions 40 and 5) for two minor purposes: (1) to aid with language polishing, and (2) to assist in the retrieval and discovery of related work. The models were not used for idea generation, analysis, or writing substantive parts of the paper.

A.2 LIMITATIONS

SYNTHESIS FEASIBILITY

Although most generated pseudo-NPs are structurally valid according to RDkit, many can be synthetically infeasible (Gao & Coley, 2020). Existing synthesis tools (e.g., AiZynthFinder, Chemformer, IBM RXN, Merck Synthia, ASKCOS) are designed for small synthetic molecules and perform poorly on the structurally rich, sp³-heavy space of NPs. We therefore acknowledge the limitation of not being able to assess the real-world synthesizability of the generated pseudo-NPs directly. Future collaborations in chemoenzymatic synthesis and protein design (e.g., NRPS for peptides) are needed to bridge this gap between computational generation and experimental synthesis. For completeness, we still report the synthetic accessibility evaluation of generated pseudo-NPs in Section A.11.

DATA AVAILABILITY

Another limitation is the lack of sufficiently large NP-only property prediction datasets, which can result in constraints in model assessment. While several NP databases exist, many rely on machine learning (ML) model-predicted rather than experimentally validated properties, and those with assay data are often too heterogeneous or fragmented to be useful for ML tasks (see Section A.3.2 for details). This lack of standardized, high-quality datasets limits both model benchmarking and evaluation.

MODEL SIZE AND ARCHITECTURE

Finally, the study does not explore how differences in model size, such as those among Mamba, Mamba-2, and GPT, might impact performance; prior work suggests observed differences may partly reflect parameter count disparities (Kaplan et al., 2020; Ross et al., 2022). While our hyperparameter search favored larger Mamba configurations, a broader comparison across CLMs (Table 4) shows that smaller models such as ChemBERTa-77M-MTR achieved competitive results despite having fewer parameters, suggesting that scale alone does not explain performance. More systematic work is needed to disentangle the trade-off between architecture, pre-training dataset size, and parameter count.

Table 4: **Model parameters and pre-training dataset size.** Model parameters are counted by summing all elements in the tensors returned by model.parameters().

Model	Parameters	Pre-training Dataset Size
ChemBERTa-77M-MLM	3.4M	77M
ChemBERTa-77M-MTR	3.4M	77M
MoLFormer-XL-both-10pct	44.4M	110M
M1-AIS-rds	59.1M	1 M
M1-npbpe1000-rds	39.8M	1 M

A.3 DATA

A.3.1 PRE-TRAINING DATA

The pre-training dataset adopted in this study has been collected from three NP databases: SuperNatural 3.0 (Gallo et al., 2022), COCONUT (Sorokina et al., 2021), and Lotus (Rutz et al., 2022). Duplicate molecules were removed, and the ones flagged by RDKit for the following structural issues were also eliminated: explicit valence issues, kekulization problems, sanitization errors, ambiguous stereochemistry, and hydrogen atoms without neighbors. Subsequently, the remaining SMILES strings in the dataset were standardized and canonicalized using RDKit's rdMolStandardize¹⁰ module to remove small fragments, normalize functional groups, and reionize molecules. Charge neutralization is then applied to adjust charged species, followed by tautomer canonicalization to ensure consistent tautomeric forms. These cleaning steps ensure the remaining dataset contains valid and interpretable molecular structures. After removing 4811 molecules that overlap with the downstream task data, the final curated pre-training NP dataset contains 1,030,273 SMILES strings, including around 21% common to all three sources and a notable overlap of almost 54% of the data points shared between COCONUT and Supernatural 3.0. This combined dataset is referred to as the 1M NP dataset throughout this study. More information regarding its feature distribution can be found in Figure 9.

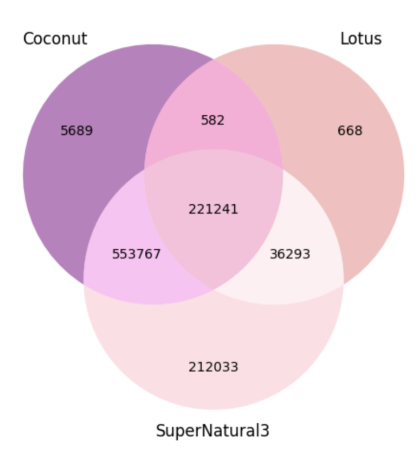


Figure 5: Pre-training data composition Venn diagram.

A.3.2 NP DOWNSTREAM DATASET AVAILABILITY AND TASK SELECTION

To the best of our knowledge, few classification datasets exist for NP molecule property prediction. The Cyclic Peptide Membrane Permeability Database (CycPeptMPDB)¹¹ is one of the few, given that peptides are a subset of NPs. Several NP databases, such as SuperNatural 3.0¹², NPASS¹³, and the Natural Products Atlas¹⁴, include properties of NP molecules, but they are primarily predicted values from ML algorithms rather than carefully curated assay results. This is problematic and not ideal in our use case, as using model-predicted feature values as input for new models can propagate existing bias. Other NP databases, such as the Comprehensive Marine Natural Products Database (CMNPD)¹⁵ and Taiwan Database of Extracts and Compounds (TDEC)¹⁶, contain assay results. However, their assay results come from various laboratories for different activity types, cell lines, and targets, and filtering them by the source, activity, cell line, and target renders the dataset

¹⁰https://www.rdkit.org/docs/source/rdkit.Chem.MolStandardize.rdMolStandardize.html
11http://cycpeptmpdb.com/
12https://bioinf-applied.charite.de/supernatural_3/
13https://bidd.group/NPASS/about.php
14https://www.npatlas.org/
15https://www.cmnpd.org/

¹⁶https://tdec.cmu.edu.tw/index_en.aspx#

too small for machine learning tasks. Thus, it is not feasible to curate meaningful NP property prediction datasets from these databases.

Nevertheless, based on the common biological activities of NPs, such as being a rich source of anti-cancer drugs and their evolutionary influence on taste and smell perception, which organisms, including humans, have relied on to select food and navigate the environment (Firn, 2009), we have chosen FourTastes and anti-cancer activity, besides the peptide membrane permeability data, as the downstream property prediction tasks. Although most of these datasets do not consist exclusively of NPs, they likely contain a higher proportion of them.

Table 5	Dataset	size	and 1	abel	distribution.

Dataset	Total Data Points	Label Distribution
Peptide Permeability	6651	$LogP_{exp} \ge -5.5$ 2836 (42.64%)
r epilae r ermeasinty	0021	$LogP_{exp} < -5.5$ 3815 (57.36%)
		Sweet 1831 (41.32%)
FourTastes	4431	Bitter 1776 (40.08%)
rourrastes	4431	Other 635 (14.33%)
		Umami 189 (4.27%)
Anti-Cancer	26039	Inactive 14548 (55.87%)
Anti-Cancer	20039	Active 11491 (44.13%)

A.3.3 PEPTIDE PERMEABILITY

Peptides constitute a subset of NPs. In the 1M NP dataset, peptides account for approximately 2% of the total compounds, with the majority originating from the Lotus database. The peptide permeability classification dataset used in this study was curated by Feller & Wilke (2025) from the Cyclic Peptide Membrane Permeability Database (CycPeptMPDB), a database compiling membrane permeability data for cyclic peptides (Li et al., 2023a). CycPeptMPDB aggregates information on 7,334 cyclic peptides from various papers and pharmaceutical patents. To refine the dataset, Feller and Wilke included only peptides with results from the Parallel Artificial Membrane Permeability Assay (PAMPA), excluding data from cell-based permeability assays. Data points that were categorized as undetectable were also removed to ensure permeability predictions were based on a more reliable and consistent subset of data. The dataset was further processed into a binary classification format using a $10^{-5.5} \log P_{\rm exp}$ threshold. Peptides with values below this threshold were classified as nonpermeable, while those at or above this value were classified as permeable. The current study has further removed 50 peptides because they overlap with the 1M NP training data, resulting in a final dataset comprising 6,651 cyclic peptides. Despite its small size, it is made of NPs entirely and has a relatively balanced label distribution, as shown in Table 5.

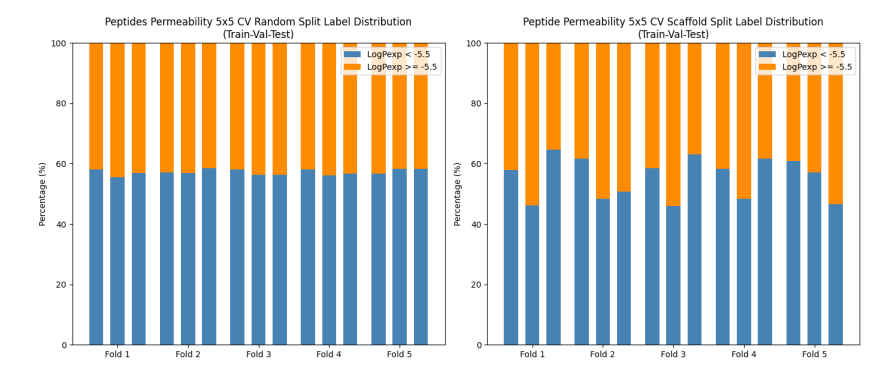


Figure 6: Peptide permeability dataset 5x5 CV random and scaffold split label distribution.

A.3.4 FOURTASTES

The FourTastes dataset is a tastes prediction dataset curated from UMP442, ChemTastesDB, and various previous literature by Androutsos et al. (2024). The dataset includes four taste labels: "sweet",

 "bitter", "umami", and "other". After preprocessing and removing overlapping data points, the final dataset consists of 4,431 data points. This dataset can be comparatively more relevant for NPs, as taste perception can be closely linked to their chemical properties. Natural compounds, such as alkaloids and flavonoids, also contribute to specific taste profiles. For example, caffeine, a kind of alkaloid, is responsible for the bitterness in coffee, while flavonoids like catechins in green tea contribute to astringency and bitter notes.

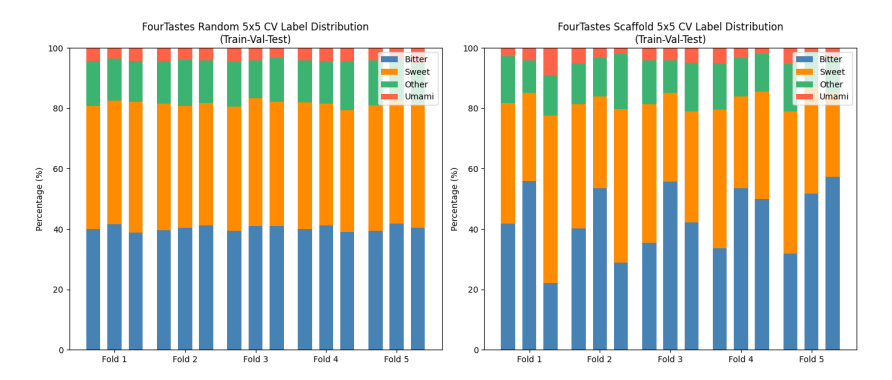


Figure 7: FourTastes dataset 5x5 CV random and scaffold split label distribution.

A.3.5 ANTI-CANCER ACTIVITY

The anti-cancer activity dataset is a binary classification dataset that differentiates between active and inactive compounds based on their ability to inhibit cancer growth. This dataset contains approximately 28,000 data points. It was initially curated by Li & Huang (2012) and extended by Al-Jarf et al. (2021), using the same curation method. The data used in this study is obtained from the pdCSM-cancer website¹⁷. The original source of the data is the NCI-60 Development Therapeutics Project (DTP), which screens small molecules against over 60 human cancer cell lines derived from nine tumor types. The bioactivity classification was determined using growth inhibition percentages (GIPRCNT) at a dose of 10^{-5} M. Compounds were classified as inactive if the average growth inhibition rate was lower than 5% (GIPRCNT>95%) in One Dose assays and active if the average inhibition rate was higher than 50% (GIPRCNT<50%) in Dose Response assays.

This dataset is valuable for its large size and standardized assay conducted by a single institution, ensuring relatively high-quality and reliable experimental results. However, it does not differentiate activity by cancer type. In real-world applications, cancer treatments are usually developed for specific tumor types. While this approach allows for the identification of broad-spectrum anti-cancer compounds, it risks missing those that have strong efficacy limited to particular cancer types.

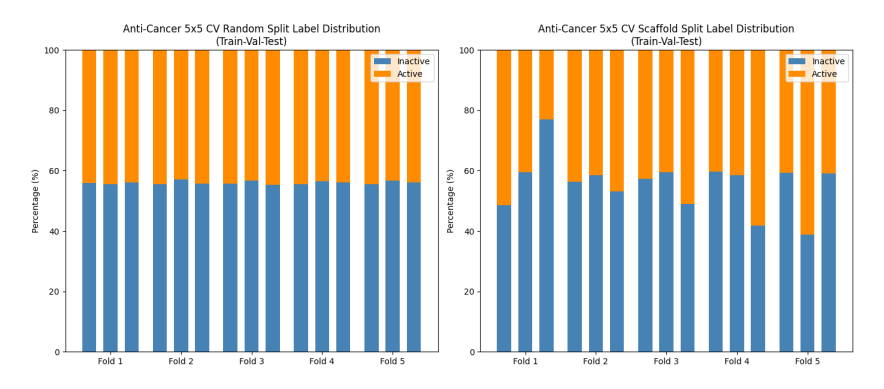


Figure 8: Anti-cancer activity dataset 5x5 CV random and scaffold split label distribution.

¹⁷https://biosig.lab.uq.edu.au/pdcsm_cancer/

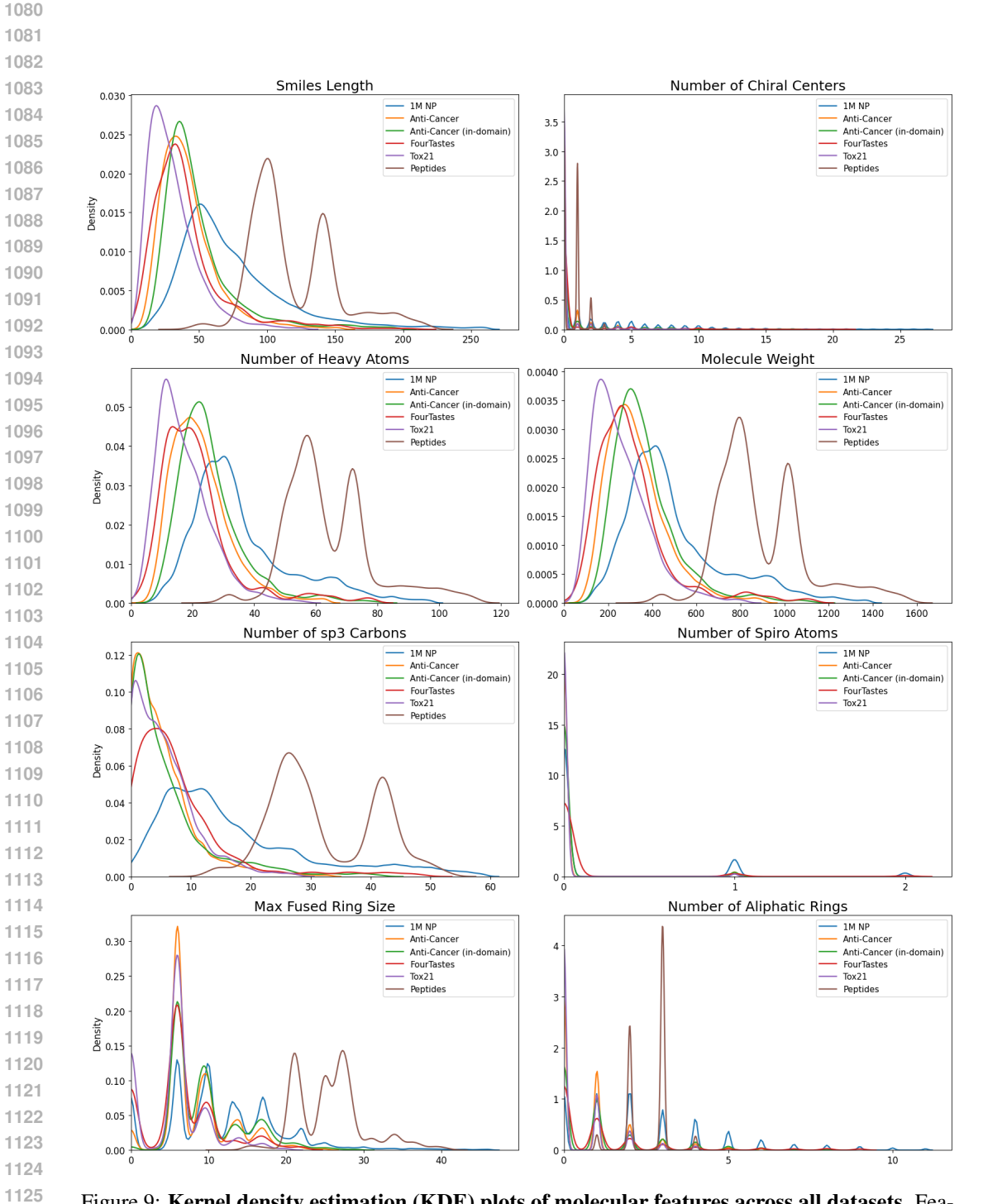


Figure 9: **Kernel density estimation (KDE) plots of molecular features across all datasets.** Features are calculated using RDkit. Extreme values beyond the 99th percentile are excluded, and bandwidth is set to 1 for all features except the number of chiral centers and number of aliphatic rings, for which a smaller bandwidth of 0.5 is used. Only assigned chiral centers are included. No spiro atoms are present in the peptide permeability dataset. Integer-valued features may show KDE curves at non-integer positions due to kernel smoothing, which spreads density beyond discrete points but does not imply fractional values.

A.4 MODELS

A.4.1 GPT

The generative pre-trained transformer (GPT) model used in this study is GPT2LMHeadModel. It is a decoder-only model with a language modeling head from the GPT-2 family. It is specifically for causal sequence generation. In this study, the GPT-2 model is trained from scratch without any pre-trained weights. GPT-2's attention layer uses masked multi-head self-attention to process sequences. Self-attention allows each token to attend to previous ones, and multi-head attention splits attention into multiple subspaces for richer feature extraction. Masked (causal) attention ensures that tokens can only attend to past and present tokens, preventing information leakage from future tokens. This structure enables GPT-2 to generate text autoregressively.

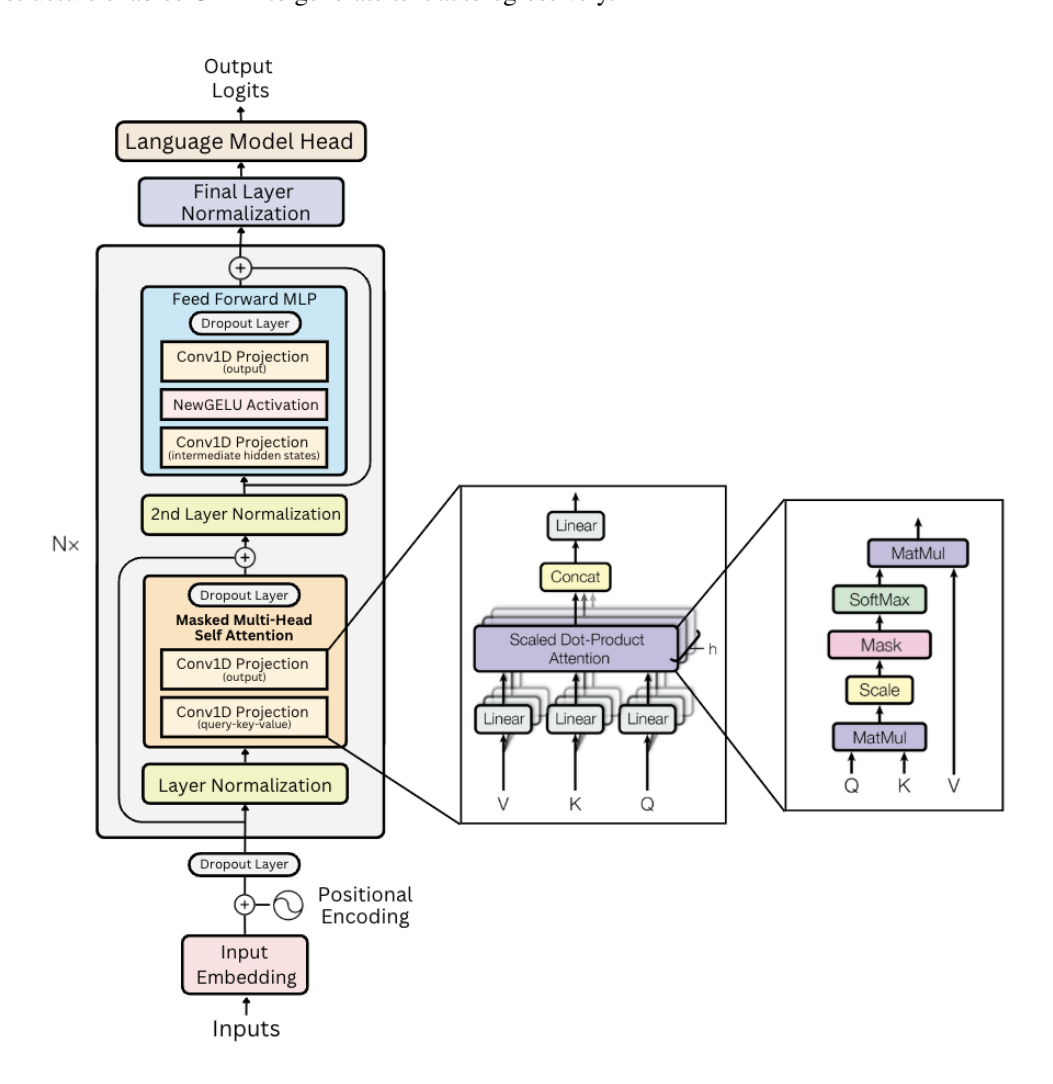


Figure 10: GPT language model architecture (adapted from Vaswani et al. (2017)).

A.4.2 MAMBA AND MAMBA-2

The Mamba model used in this study is the MambalMHeadModel, which is a Mamba backbone mixer model with a language modeling head. Both Mamba and Mamba-2 share the same overall architecture. They differ only in the mixer component. The overall structure of the Mamba model and its components is illustrated in Figure 13. The main difference between Mamba and Mamba-2's neural network architecture is that the SSM parameters, A, B, and C in Mamba-2 are produced in parallel with the X input instead of sequentially as in Mamba (Dao & Gu, 2024). The input is first

 turned into embeddings and then passes through a varying number of blocks (N) containing Mamba blocks before reaching the final language modeling head for the final output.

Mamba is a sequence model that achieves high modeling quality on dense modalities while addressing transformers' inefficiency in handling long sequences (Gu & Dao, 2024). It builds on the S4 model, a type of SSMs, which employs time-invariant dynamics and performs well on continuous data such as audio. SSMs have been less effective with discrete data types because their fixed, uniform processing does not account for how each token's importance at a certain step can change depending on the surrounding tokens in a sequence (Gu & Dao, 2024); for example, like in text or SMILES strings, related tokens may be far apart in a sequence, creating long-range dependencies that are more challenging to capture. To address this limitation, Mamba has introduced selective SSMs (S6), which dynamically adjust parameters (Δ , B, and C) based on input (see Figure 11). This time-variant nature allows better content-aware processing. Yet, it complicates convolutionlike operations and parallelization. To overcome this, Mamba adopts a parallel scan algorithm and hardware-aware optimizations like kernel fusion and recomputation to greatly improve efficiency on GPUs. Unlike transformers, which store full sequence context through key-value caches, making them computationally heavy, Mamba filters and propagates information more efficiently with input-dependent recurrence (Gu & Dao, 2024; Vaswani et al., 2017). Mamba's design enables faster training and inference on longer sequences than transformers, while achieving lower perplexity and strong performance, especially in bioinformatic and cheminformatic tasks (Gu & Dao, 2024; Brazil et al., 2024; Xu et al., 2024; Thoutam & Ellsworth, 2024; Sgarbossa et al., 2024; Peng et al., 2024).

Mamba-2 builds on Mamba's architecture with a structured state space duality (SSD) framework, showing that SSMs and causal linear attention can be represented as semi-separable matrices (Dao & Gu, 2024). This allows for efficient intra- and inter-chunk computations. By incorporating optimization techniques like tensor and sequence parallelism, Mamba-2 has been reported to further improve hardware efficiency, achieving 2 to 8 times faster training than Mamba, while maintaining transformer-level performance (Dao & Gu, 2024). However, it simplifies the SSM parameter A to a scalar-times-identity form and generates parameters A, B, and C in parallel from input X (instead of sequentially like in Mamba (see Figure 12), reducing contextual sensitivity and potentially limiting model expressiveness (Dao, 2024).

Selective State Space Model with Hardware-aware State Expansion A A A A Bt Discretis Selection Mechanism GPU HBM Selection Mechanism

Figure 11: **Selective SSM** (S6) maps an input x to an output y by transitioning through a higher-dimensional latent state h, utilizing time-variant, input-dependent parameters Δ , B, and C (A being affected indirectly via discretization with Δ) with an algorithm optimized for efficient use of GPU memory hierarchy levels (Gu & Dao, 2024).

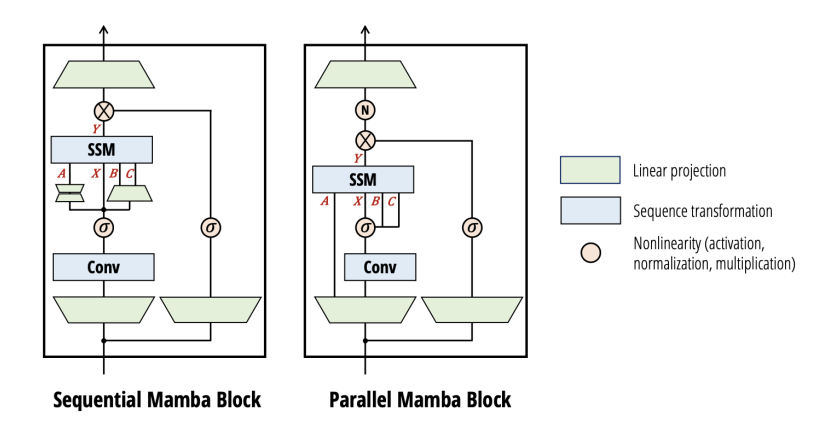


Figure 12: **Sequential and parallel mamba blocks.** The Mamba-2 block (right) simplifies the original Mamba block (left) by generating SSM parameters (A, B, and C) directly from the input X in parallel at the start of the block instead of computing them sequentially as functions of the input X, thereby making it more suitable for scaling method such as tensor parallelism (Dao & Gu, 2024; Dao, 2024).

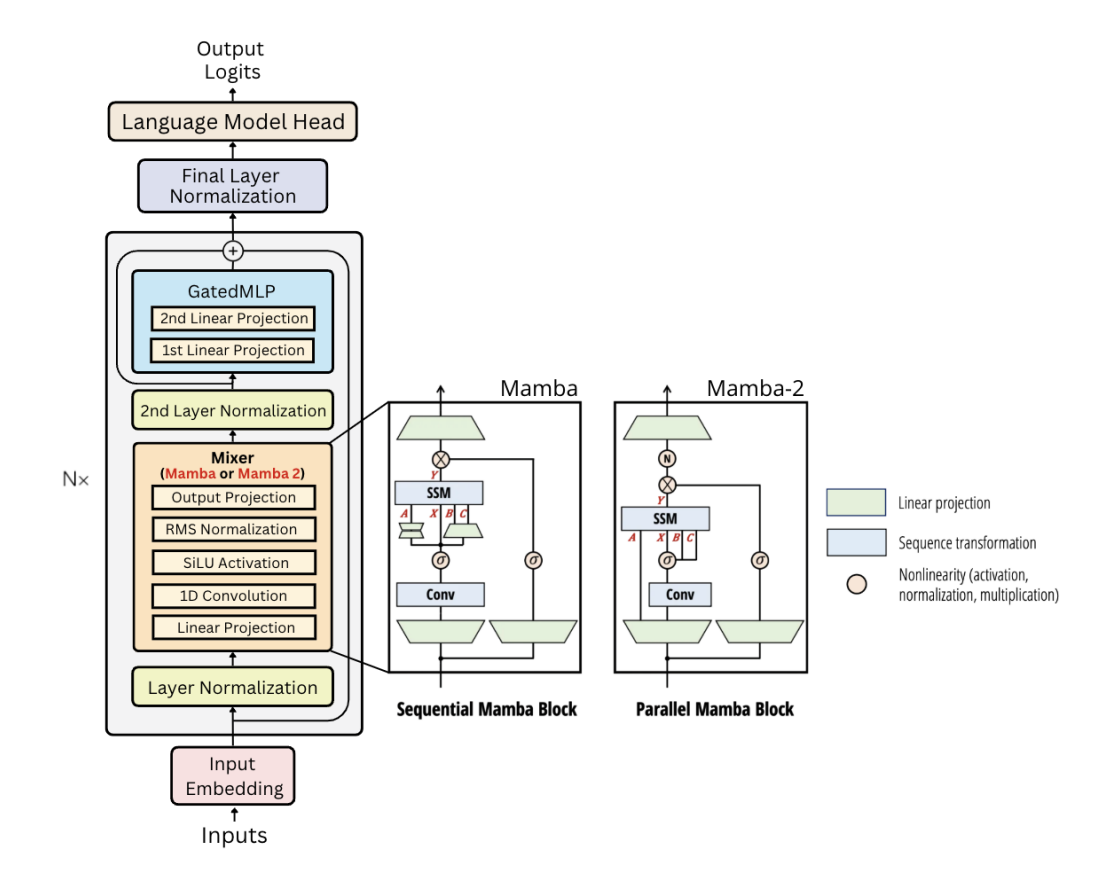


Figure 13: Mamba language model architecture (adapted from Gu & Dao (2024); Dao & Gu (2024)).

A.4.3 MOLFORMER

MoLFormer is an encoder-only transformer-based CLM designed to capture chemical representations from SMILES sequences using rotary positional embeddings, a linear attention mecha-

Table 6: Comparison of Mamba and Mamba-2 (Dao, 2024).

Feature	Mamba	Mamba-2		
SSM Design	Diagonal structure, independent channel control.	Scalar-times-identity structure, uniform dynamics.		
Hardware Efficiency	Less optimal matrix utilization.	Optimized matrix multiplications for GPUs/TPUs.		
Theoretical Framework	No structured duality framework.	Introduces SSD, linking SSMs and attention mechanisms.		
Head Dimension	Single head per channel.	Larger head dimensions (e.g., 64), shared dynamics across channels.		
State Dimension	Smaller (e.g., N=16), limited scalability.	Larger (e.g., N=64 to N=256), enhances scalability and training speed.		
Efficiency & Scalability	Flexible control, less training efficiency.	Highly efficient in training, streamlined structure.		
Training vs. Inference	Assumed better inference per- formance (more expressive) due to flexibility.	Fast training optimized (sequences longer than 2K), maintains efficient inference.		

nism, and Regex-based tokenization (Ross et al., 2022). The Molformer-XL has been pretrained on 1.1 billion unlabelled molecules from the PubChem and ZINC databases. The PubChem database includes a wide range of chemical substances, from small molecules to larger macromolecules, while the ZINC database focuses on offering commercially available compounds curated for virtual screening. The Molformer model utilized in this study is one of its variants, the Molformer-XL-both-10pct, which has been trained on a 10% subset from both the PubChem and ZINC datasets. Results indicate that the Molformer-XL-both-10pct variant performed very close and only slightly inferior to the full-scale Molformer-XL, which has been trained on a dataset ten times larger.

Fine-tuning MoLFormer on the random split 1M NP dataset uses the same MLM pre-training objective. The 1M NP dataset is tokenized using the same tokenizer from MoLFormer, resulting in a total of 149 tokens. To identify optimal hyperparameters, 5% of the training and validation data were used for hyperparameter tuning with Optuna, testing learning rates between 1e-5 and 5e-5 and batch sizes of 8, 16, and 32 over 10 trials. The best-performing configuration was then used for full fine-tuning, employing weight decay with early stopping based on validation loss, with a patience value of 5 epochs to prevent overfitting. The final model was evaluated on a held-out test set. After fine-tuning on 1M NPs, the MoLFormer model is adapted for classification by adding a dropout layer (dropout rate = 0.1) and a randomly initialized fully connected linear layer as the classification head. The sequence representations from the last hidden state are extracted as a summary of the entire sequence that is later fed into a classification head to learn task-specific features and generate predictive outputs.

A.4.4 CHEMBERTA-2

ChemBERTa-2 is a RoBERTa-based transformer model built upon ChemBERTa (Ahmad et al., 2022). Its pre-training dataset consists of 77 million unique SMILES strings sourced from Pub-Chem, which includes a diverse range of small molecules as well as larger natural and chemically modified compounds such as nucleotides, carbohydrates, lipids, and peptides. The multi-task regression (MTR) version of ChemBERTa-2 generally outperforms the MLM version on downstream tasks. The MLM variant has been chosen for fine-tuning on 1M NPs in this case because it is less computationally expensive and time-consuming, as the MTR variant requires extracting 200 molecular features per data point, leading to large feature vectors that substantially increase training time.

1351

1352

1353

1354

1355

1356

1357

1358

1359

1360

1361

1362

1363

1364

1365

1368

1369

1370

1371

1372 1373

1374 1375

1376

1377

1378

1379

1380

1381

1382

1383

1384

1385

1386

1387

1388

1389

1390

1391

1392

1393

1394

1395

1396

1398

1400

1401

1402

1403

The MTR variant is, however, deployed for the downstream property prediction task directly without being fine-tuned on 1M NPs.

One important limitation worth mentioning is that ChemBERTa models have several tokenizer-related issues. A particularly relevant one in this case is that it cannot distinguish chiral centers, yet they are prevalent in NPs. When encountering chiral notations like [C@@H] and [C@H], the ChemBERTa-2 tokenizer tokenizes them into simply "C," effectively losing stereochemical information. Due to this limitation, applying ChemBERTa-2's tokenizer to the 1M NP dataset produces only 32 unique tokens, which is even less than the vocabulary size of the character-level tokenizer in this study. This can impact the model's ability to differentiate structural features. Further discussion on this topic can be found in Section A.6.5.

Fine-tuning ChemBERTa-2 (ChemBERTa-77M-MLM) adopts the same pre-training MLM objective, and the fine-tuning process is the same as that of MoLFormer. The 1M NP dataset is tokenized with the original ChemBERTa-2's tokenizer. The hyperparameter search uses 5% of the training and validation data with Optuna, with a search space of learning rates between 1e-5 and 5e-5 and batch sizes of 8, 16, and 32 over 10 trials. The best configuration was used for full fine-tuning with weight decay and early stopping (patience = 5 epochs) based on validation loss. After ChemBERTa-77M-MLM is fine-tuned on 1M NPs, it is then adapted for property prediction tasks by adding a classification head consisting of a dropout layer (dropout rate = 0.1) and a randomly initialized fully connected linear layer, the same as all other models. The forward pass extracts the contextualized representation of each sequence, namely, using the [CLS] token embedding, which is the first token embedding from the last hidden state. During fine-tuning for property prediction tasks, the model learns to encode task-relevant features into this embedding, making it a meaningful sequence summary representation for classification.

A.5 RELATED WORK (EXTENDED)

NIMO, developed by Shen et al. (2024), is a transformer-based model designed for NP-inspired molecular generation. It employs a motif-based representation with custom fragmentation methods to preserve stereochemical information and enhance structural design. Trained on datasets that are mostly NPs, including COCONUT, ChEMBL, and TeroKIT, NIMO has shown success in generating diverse, drug-like molecules with high structural relevance. **NPGPT** is developed by Sakano et al. (2024) for NP-like molecular generation. The authors fine-tuned SMILES-GPT (GPT-2-based) and ChemGPT (GPT-Neo-based) models on around 400,000 NPs from the COCONUT database, which was then expanded to around 3.6 million molecules through augmentation. The augmentation process involved enumerating multiple valid SMILES representations for the same molecule by altering the traversal order of atoms during encoding. The fine-tuned models generated molecules that closely matched real NPs in terms of molecular weight, stereochemistry, and NP-likeness. The study also demonstrates how deep learning can accelerate NP-based drug discovery by efficiently navigating complex chemical spaces. Feller & Wilke (2025) have introduced **PeptideCLM**, a transformer-based CLM designed to predict the membrane permeability of cyclic peptides, a subset of NPs with significant pharmaceutical potential. The authors used a pre-training dataset of 23 million molecules, including 10 million small molecules from PubChem, another 2.2 million small molecules from SureChEMBL, 825,632 natural peptides, and 10 million synthetic peptides. The models reportedly address limitations in peptide representation using a custom tokenization strategy based on SMILES Pair Encoding (SPE) within a BERT-style architecture, and they have been successfully applied to predict peptide permeability. Tay et al. (2023) trained a recurrent neural network (RNN) with long short-term memory (LSTM) units using the COCONUT database, which contains approximately 406,000 NP molecules. They applied SMILES enumeration to augment the training dataset, expanding it to around 3.25 million entries, following a similar approach to what Sakano and Furui have adopted. Using this model, they generated 100 million molecules, of which around 67 million were unique and valid. Their findings indicate that the generated compounds expand the known chemical space while preserving NP characteristics, closely resembling real NPs in NP-likeness scores and biosynthetic pathway classification, with low Kullback-Leibler (KL) divergence. Ozçelik et al. (2024) have used structured state-space sequence (S4) model, GPT, and LSTM to generate NP-like molecules, training on 32,360 data points from the COCONUT database to produce 102,400 NP-like SMILES strings de novo. They have shown that the S4 model, which is the predecessor to Mamba, can enhance the generation of NP-like molecules by generating higher percentages of diverse and structurally novel molecules compared to GPT, RNN, and LSTM.

Recent research in CLMs for NPs has demonstrated that LLMs can effectively expand the chemical space of NPs by generating NP-like molecules. However, to the best of our knowledge, no studies have investigated the use of Mamba models for NP-focused CLMs, nor have any systematically examined tokenization strategies for NPs on property prediction tasks. Furthermore, some models are pre-trained on molecular datasets that cover a broader chemical space before being fine-tuned for NPs. This prompts the question of whether it is more effective to pre-train models solely on NPs or to fine-tune existing CLMs using NP data. Therefore, this work aims to address these gaps.

A.6 TOKENIZATION

Tokenization converts molecular representations into tokens for processing by language models. SMILES tokenization differs from natural languages. Natural language tokens represent words or subwords and must handle punctuation, ambiguity, and more redundancy that come with the use of stop words. Chemical text representations like the SMILES strings, however, are designed to encode atoms, bonds, branches, and rings in a more compact way. SMILES tokenization can be character-, atom-, or motif-level (Liao et al., 2024). Character-level tokenizer treats each character as a token. Atom-level focuses on individual atoms. Motif-level uses substructures, derived either from chemical rules or subword algorithms like byte-pair encoding (BPE). While motif- and atom-level methods are more chemically grounded, character-level tokenization has also shown to be effective (Lu & Zhang, 2022). Some studies have shown that optimized tokenizers such as BPE, WordPiece, and Unigram can enhance transformer-based CLM performance while reducing input length (Dotan et al., 2024). SMILES Pair Encoding (SPE), a BPE variant, improves generation and prediction by incorporating chemical meaning (Li & Fourches, 2020). Atom-in-SMILES (AIS) includes atomic environments, outperforming character-level and SPE in property prediction tasks (Ucak et al., 2023).

A.6.1 CHARACTER-LEVEL TOKENIZER

Character-level tokenization is a straightforward method that divides SMILES strings into individual characters, sometimes leading to separation of multi-character units. However, research has shown its effectiveness in some CLMs (Liao et al., 2024). Tokenizing the 1M NP dataset by the character-level tokenizer results in a vocabulary size of 48, including four special tokens (padding, unknown, beginning, and end of sequence tokens).

A.6.2 DEEPCHEM BYTE-PAIR ENCODING (BPE) TOKENIZER

The tokenizer sourced from DeepChem (seyonec/PubChem10M_SMILES_BPE_450k ¹⁸) is a BPE tokenizer with a vocabulary size of 7,924 tokens. In this study, this tokenizer is simply referred to as "BPE." This tokenizer is not specifically tailored for NPs. Therefore, when applied to 1M NPs, only about 1,700 out of the total 7,924 tokens are included, and much of the tokenizer's broader vocabulary remains unused.

A.6.3 ATOM-IN-SMILES (AIS) TOKENIZER

The atom-level tokenizer adopted in this study is the Atom-in-SMILES (AIS) tokenizer developed by Ucak et al. (2023). It is a tokenization scheme designed to address limitations in traditional SMILES tokenization by including an atom's local chemical context or atom environments (AEs) in its token. AIS tokenization can also mitigate token degeneration issues by reducing token repetition. The AIS algorithm processes the input strings by first parsing the SMILES string into a chemical graph, identifying atoms and bonds. It then analyzes each atom's local chemical environment by detecting neighboring atoms within a specific bond radius, examining bond types, and capturing features like aromaticity, chirality, and hybridization. Based on this analysis, AIS generates context-aware tokens for each atom, incorporating the central atom, neighboring atoms, bond types, and special chemical properties. For example, the AIS tokenization output of ethanol's SMILES string "CCO" are "[CH3;!R;C], [CH2;!R;CO], [OH;!R;C]," where [CH3;!R;C] denotes a methyl group not in a ring, bonded to a carbon; [CH2;!R;CO] is a methylene group not in a ring, bonded to a carbon.

¹⁸https://huggingface.co/seyonec/PubChem10M_SMILES_BPE_450k

Tokenizing the 1M NP pre-training dataset by the AIS tokenizer results in a vocabulary size of 1023, including the special tokens. It is also important to note that the AIS tokenizer may occasionally interchange the counterclockwise ("@") and clockwise ("@") chiral designations when mapping SMILES to AIS tokens. This phenomenon arises from RDKit's internal processing of chiral centers, where chirality is assigned based on the atom's local environment.

A.6.4 NATURAL PRODUCT BYTE-PAIR ENCODING (NPBPE) TOKENIZER

The Natural Product Byte-Pair Encoding (NPBPE) tokenizers are made specifically for NPs. They are trained using the tokenizers.trainers.BpeTrainer class from Hugging Face on the 1M NP dataset. The process involves using a pre-tokenizer that isolates individual SMILES characters and then iteratively merges frequent character pairs to create more extended units. Five distinct NPBPE tokenizers are created by setting maximum vocabulary sizes to 60, 100, 1000, 7924, and 30,000 tokens (including special tokens).

Table 7: Examples of tokenized SMILES strings for each tokenizer.

Example SMILES:	CC1=C2[C@@H]3[C@H](C(:	=0)C1)[C@@]	2 (C) CCCC3 (C)	С
-----------------	-------------	-------------	-------------	-----------------	---

Examp	le SMILES: CC1=C2[C@@H]3[C@H](C(=O)C1)[C@@]2(C)CCCC3(C)C
Tokenizer	Tokens
Character- level	C, C, 1, =, C, 2, [, C, @, @, H,], 3, [, C, @, H,], (, C, (, =, O,), C, 1,), [, C, @, @,], 2, (, C,), C, C, C, C, 3, (, C,), C
AIS	[CH3;!R;C], [C;R;CCC], 1, =, [C;R;CCC], 2, [[C@H];R;CCC], 3, [[C@H];R;CCC], (, [C;R;CCC], (, =, [O;!R;C],), [CH2;R;CC], 1,), [[C@@];R;CCCC], 2, (, [CH3;!R;C],), [CH2;R;CC], [CH2;R;CC], [CH2;R;CC], [C;R;CCCC], 3, (, [CH3;!R;C],), [CH3;!R;C]
BPE	CC, 1, =, C, 2, [, C, @, @, H,], 3, [, C, @, H,](, C, (=, 0,), C, 1,)[,C, @, @,], 2, (, C,), CCCC, 3, (, C,), C
NPBPE60	CC, 1, =, C, 2, [C@, @, H,], 3, [C@, H,], (, C(, =, O), C, 1,), [C@, @,], 2, (, C,), CC, CC, 3, (, C,), C
NPBPE100	CC1, =, C2, [C@@H], 3, [C@H](, C(=O), C1,), [C@@], 2, (C), CCCC, 3, (C), C
NPBPE1000	CC1=C2, [C@@H]3, [C@H](, C(=O), C1), [C@@]2(C), CCCC, 3(C), C
NPBPE7924	CC1=C2, [C@@H]3[C@H](, C(=O), C1), [C@@]2(C), CCCC3(C), C
NPBPE30k	CC1=C2, [C@@H]3[C@H](, C(=O), C1), [C@@]2(C), CCCC3(C)C



Figure 14: **Jaccard similarity between tokenizers.** The Jaccard similarity is calculated by dividing the size of each tokenizer pair's token intersection by the size of their union; for BPE, only the tokens actually used in 1M NPs (approximately 1,700) are included.

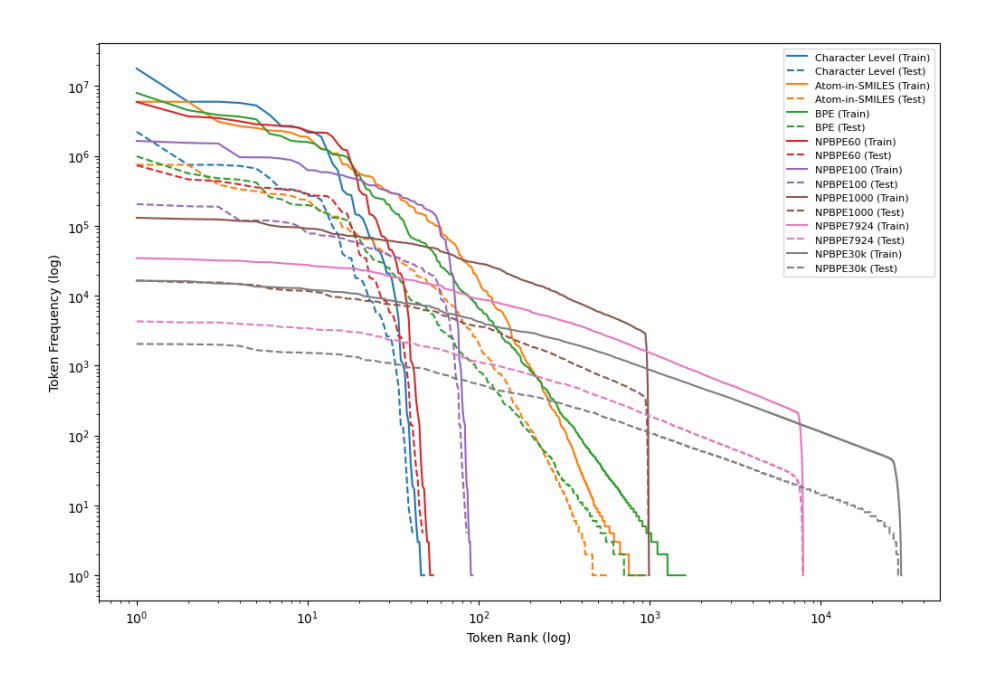


Figure 15: **Zipfian distributions of tokens generated by each tokenizer.** The training and testing sets shown in the plot are the scaffold split subsets of the 1M NP dataset.

A.6.5 WHEN TOKENIZATION FAILS....

MoLFormer's fine-tuning on 1M NPs took approximately 10 days, whereas ChemBERTa-77M-MLM completed fine-tuning in about 12 hours. Although differences in architecture and model size likely contribute to this discrepancy, another possible factor is the diversity of their tokenizer outputs: ChemBERTa-2's tokenizer generated only 32 distinct tokens from the 1M NP dataset, in contrast to MoLFormer's 149. This disparity results from known tokenization issues in ChemBERTa models—for example, stereochemical details are simplified to basic tokens, and bracketed annotations and charge indicators are omitted—causing distinct SMILES components to become identical tokens. Although the impact of this tokenizer issue on training and inference performance has not

been formally assessed, it can already be observed that ChemBERTa-77M-MLM, both its fine-tuned and non-fine-tuned versions, consistently underperform compared to all other models in this study. This result aligns with the ChemBERTa-2 paper, which also reports the superior performance of the multi-task regression (MTR) variant over MLM. It should be noted that ChemBERTa-2's MTR pre-trained variant also has the same tokenization issue. However, despite this issue, it still performs reasonably well compared to other models without tokenizer issues. One can perhaps speculate that the MTR pre-training objective may be inherently more resilient to poor tokenization than MLM. While MLM relies heavily on token-level relationships, requiring precise tokenization to reconstruct masked tokens, MTR leverages 200 precomputed molecular features calculated directly from SMILES strings, and the model has been trained to predict all 200 properties simultaneously (Ahmad et al., 2022). These numerical features, derived using RDKit, provide chemical contexts that allow the model to focus on molecular features and not rely solely on token-level granularity. As a result, MTR pre-training can perhaps be less dependent on the quality of tokenized input and more driven by the underlying chemical patterns and relationships embedded in numerical descriptors, thereby enabling the model to learn more robust, chemically grounded representations even when tokenized input is suboptimal. Nonetheless, this remains a speculation, and further research is necessary to determine the exact mechanisms behind this robustness and whether fixing the tokenizer could enhance the MLM variant's performance.

A.7 FINE-TUNING ON DOWNSTREAM TASKS

Hyperparameter optimization is performed using only the training and validation subsets. Each fold undergoes a full fine-tuning process for three epochs, and the evaluation metric is recorded after the third epoch. The evaluation results for all 5 folds are then averaged. This process is repeated for each of the six hyperparameter combinations in the search space (learning rates: 1e-4, 1e-5, 5e-5; batch sizes: 8, 16). The combination resulting in the highest average performance across the 5 folds on the validation data is selected for fine-tuning. Figure 16 illustrates the hyperparameter search process for all property prediction tasks in this study.

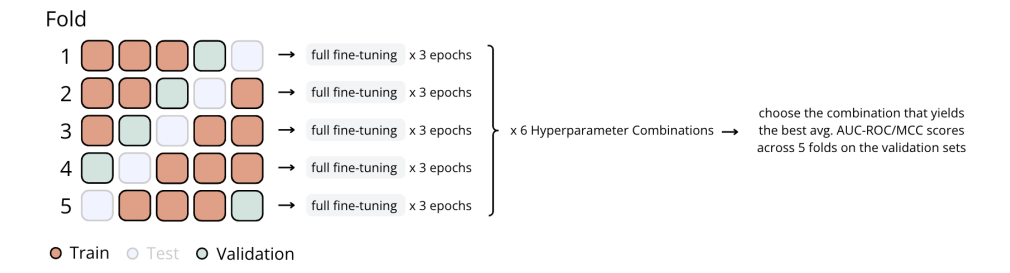


Figure 16: 5×5-fold cross-validation - hyperparameter search.

Fine-tuning on property prediction tasks is performed using full fine-tuning on each fold, with early stopping applied with the patience value set to 5 epochs. This fine-tuning process is repeated 5 times per fold, with each repetition starting from the original model weights (i.e., prior to any modifications using the downstream task data). The test results from these 5 repetitions per fold are averaged to obtain a more reliable performance estimate. After all 5 folds have been processed, the final results are computed by averaging the respective fold-wise outcomes, along with the corresponding standard deviation and standard error (SE). This repeated 5×5-fold cross-validation fine-tuning process is illustrated in Figure 17.

Loss functions for each task differ slightly. For the FourTastes dataset, CrossEntropyLoss() is used for multi-class classification, as the task involves four taste categories. This loss function applies a softmax activation to convert logits into class probabilities. Due to the highly imbalanced label distribution, class weighting is applied to mitigate class imbalance. The class weights are computed using compute_class_weight() from sklearn and incorporated into the loss function, ensuring higher loss penalties for underrepresented classes. For the anti-cancer activity and peptide permeability datasets, class distributions are approximately balanced; thus, no class weighting is applied. These two binary classification tasks use the BCEWithLogitsLoss() function, which combines a sigmoid activation with binary cross-entropy loss.



Figure 17: 5×5-fold cross-validation - fine-tuning.

Table 8: **Model performance comparison** for anti-cancer activity (MCC±SE) and peptide permeability (AUC-ROC±SE). This table presents the same results as those shown in Figure 4, but rendered in tabular form for clarity.

		Fine-tune	d on 1M NPs	Pre-trained on 1M NPs
		ChemBERTa- 77M-MLM	MoLFormer-XL- both-10pct	NP Mamba (M1-AIS-rds)
Anti-Cancer	Random	0.779±0.004	0.810±0.003	0.814±0.003
Activity	Scaffold	0.638±0.023	0.681±0.021	0.673 ± 0.020
Peptide	Random	0.847±0.005	0.855±0.006	0.863±0.004
Permeability	Scaffold	0.755±0.018	0.759 ± 0.027	0.777 ± 0.013
		W	ithout Fine-tuning	on 1M NPs
		ChemBERTa- 77M-MLM	MoLFormer-XL- both-10pct	ChemBERTa- 77M-MTR
Anti-Cancer	Random	0.777±0.001	0.814±0.002	0.806±0.003
Activity	Scaffold	0.633±0.019	0.689 ± 0.021	0.680 ± 0.026
Peptide	Random	0.845±0.005	0.855±0.005	0.863±0.004
Permeability	Scaffold	0.751±0.018	0.732 ± 0.031	0.775 ± 0.018

Figure 18 presents the multiple comparisons similarity (MCSim) plots for the FourTastes results under both random and scaffold splits using random split pre-trained models, providing easier pairwise comparisons and highlighting statistically significant differences. The MCSim plots show that differences between tokenizers are more pronounced than between models, and tokenizers using larger NPBPE vocabularies perform significantly worse than most other tokenizers.

A.8 MOLECULE GENERATION DETAILS

Molecule generation is conducted using an autoregressive sampling approach with a temperature of one, which means the model samples directly from its learned probability distribution. Each of the 48 model variations generates 100,000 molecules in a batch-wise manner, with a maximum sequence length of 512 tokens and a batch size of 32. Generation begins with a start-of-sequence token and proceeds token-by-token, sampling from the model's probability distribution until the end-of-sequence token is reached. Generation time is recorded for performance assessment. The generated molecules are evaluated for validity, uniqueness, and novelty, with their NP-likeness and SAScores compared to their respective training data (see Section A.11 for details regarding NP-likeness and SAScores). More information on molecule generation results can be found in Figures 19 and 20 below.

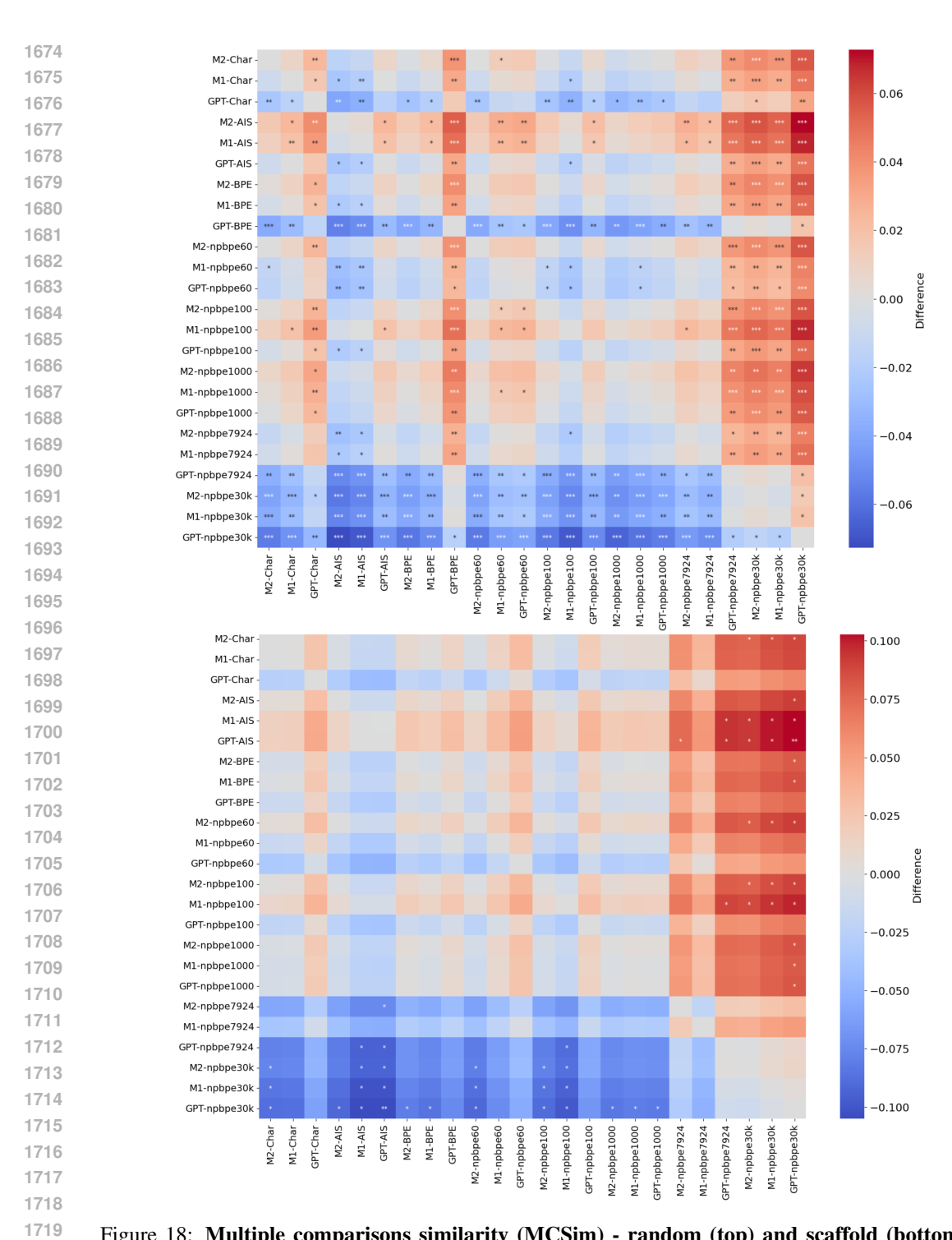


Figure 18: Multiple comparisons similarity (MCSim) - random (top) and scaffold (bottom) split FourTastes + random split pre-trained models: this heatmap visualizes pairwise differences in model performance, with statistical significance indicated by asterisks (*); pairwise comparisons are conducted using Welch's t-test, which compares means while accounting for unequal variances; degrees of freedom are estimated using the Welch-Satterthwaite equation, and two-tailed p-values are calculated using the Student's t-distribution; statistical significance is assigned based on p-values: ***(p < 0.001), **(p < 0.01), and *(p < 0.05).

	Model	Character-Level	Atom-in-SMILES	BPE	NPBPE60	NPBPE100	NPBPE1000	NPBPE7924	NPBPE30k
Tokenizer Voo	Tokenizer Vocabulary Size	48	1023	7924	09	100	1000	7924	30000
Averaged Tokenize	Averaged Tokenized Sequence Length	74.9	62.97	58.48	32.4	32.4	22.45	10.9	8.57
	M2	80.93%	81.57%	73.68%	82.03%	76.58%	80.65%	65.17%	26.98%
Valid	M	81.21%	81.89%	80.33%	79.07%	85.36%	76.96%	75.86%	57.33%
	GPT	79.91%	80.82%	80.25%	79.89%	79.86%	84.83%	64.46%	57.55%
	M2	80.08	80.49%	72.85%	81.00%	75.59%	78.97%	63.55%	54.83%
Unique	N	80.34%	80.76%	79.39%	78.16%	84.28%	75.58%	73.61%	55.13%
	GPT	79.14%	79.50%	79.12%	78.85%	78.50%	82.86%	62.02%	54.87%
	M2	70.12 / 67.94%	71.31 / 69.18%	64.17 / 62.22%	70.00 / 67.61%	69.65 / 68.20%	62.32 / 59.52%	56.09 / 54.63%	46.54 / 45.11%
Novel (train/all data)	M	70.86 / 68.73%	71.42 / 69.36%	%81.79 / 88.69	68.34 / 66.07%	71.11 / 68.34%	68.88 / 67.36%	54.30 / 51.41%	47.25 / 45.79%
(2000)	GPT	75.09 / 74.01%	74.03 / 72.70%	71.72 / 69.99%	72.21 / 70.62%	69.13 / 67.01%	69.00 / 66.01%	55.03 / 53.50%	46.39 / 44.82%
	M2	1.1088 ± 0.0046	1.1300 ± 0.0046	1.0695 ± 0.0047	1.1180 ± 0.0047	1.0898 ± 0.0046	1.1329 ± 0.0047	1.0770 ± 0.0049	0.9964 ± 0.0054
NP-Likeness	Μ	1.1204 ± 0.0046	1.1162 ± 0.0046	1.0745 ± 0.0046	1.0851 ± 0.0047	1.1145 ± 0.0045	1.0817 ± 0.0046	1.1053 ± 0.0049	1.0166 ± 0.0053
	GPT	1.0099 ± 0.0047	1.0651 ± 0.0046	0.9845 ± 0.0047	0.9773 ± 0.0046	1.1371 ± 0.0047	1.1138 ± 0.0047	0.9482 ± 0.0052	0.9930 ± 0.0054
	M2	4.2507 ± 0.0045	4.2398 ± 0.0046	4.1795 ± 0.0046	4.2305 ± 0.0045	4.2607 ± 0.0047	4.2669 ± 0.0046	4.2464 ± 0.0049	4.1652 ± 0.0053
SAScore	M	4.2822 ± 0.0045	4.1981 ± 0.0045	4.2046 ± 0.0044	4.2529 ± 0.0046	4.2984 ± 0.0046	4.3246 ± 0.0047	4.2625 ± 0.0047	4.1736 ± 0.0053
	GPT	4.2145 ± 0.0044	4.2218 ± 0.0045	4.2233 \pm 0.0044	4.2337 ± 0.0044	4.3527 ± 0.0046	4.3195 ± 0.0045	4.1050 ± 0.0048	4.1141 ± 0.0051
F	M2	0.2756 sec	0.1493 sec	0.0707 sec	0.1536 sec	0.0451 sec	0.0294 sec	0.0142 sec	0.0094 sec
(ner molecule)	M	0.1803 sec	0.1257 sec	0.1893 sec	0.0482 sec	0.0522 sec	0.0141 sec	0.0084 sec	0.0062 sec
(amagan)	GPT	0.1658 sec	0.0410 sec	0.1201 sec	0.0453 sec	0.0167 sec	0.0050 sec	0.0097 sec	0.0055 sec
;	M2	7 hr 39 min	4 hr 9 min	1 hr 59 min	4 hr 16 min	1 hr 15 min	45 min	23 min	15 min
Generation Time	M1	5 hr	3 h 29 min	5 hr 17 min	1 hr 20 min	1 hr 27 min	23 min	14 min	10 min
(1000)	GPT	4 hr 36 min	1 hr 8 min	3 hr 22 min	1 hr 15 min	27 min	8 min	16 min	9 min
	M2	42676	40497	39165	42023	43775	38908	36620	30842
Unique Scaffolds	M	43251	40844	41588	41374	44101	44929	35729	31027
	GPT	44996	38701	43364	44513	40600	40317	34151	28680
	M2	31296	28393	29783	29838	36290	24395	29493	23820
Novel Scarrols	M1	32444	29572	31182	30295	30340	37144	20885	24079
(ana) 6	GPT	37821	29898	35212	36184	30710	27148	27719	21723
(M2	31194	28279	29692	29724	36189	24300	29415	23746
Novel Scaffols	M1	32339	29463	31097	30192	30217	37051	20799	23996
(200	GPT	37740	29810	35128	36087	30609	27034	27658	21659

Figure 19: Molecule generation result table (random split pre-trained models).

Metric	Model	Character-Level	Atom-in-SMILES	BPE	NPBPE60	NPBPE100	NPBPE1000	NPBPE7924	NPBPE30k
Tokenizer Vo	Tokenizer Vocabulary Size	48	1023	7924	09	100	1000	7924	30000
Averaged Tokenized Sequence Length	d Sequence Length	74.9	62.97	58.48	32.4	32.4	22.45	10.9	8.57
	M2	82.87%	80.45%	79.50%	74.53%	79.68%	78.64%	72.99%	47.40%
Valid	M	80.45%	80.62%	79.42%	80.85%	78.92%	76.64%	67.88%	57.46%
	GPT	74.45%	82.21%	77.46%	81.76%	84.46%	83.67%	66.24%	45.89%
	M2	81.53%	79.01%	78.27%	73.50%	78.00%	76.11%	69.84%	45.25%
Unique	M	79.35%	79.30%	78.12%	79.77%	77.74%	74.74%	65.52%	54.55%
	GPT	73.62%	80.89%	76.27%	80.63%	82.61%	81.23%	63.38%	42.48%
:	M2	66.63 / 66.45%	%05'99 / 66'20%	64.73 / 64.61%	%80.99 / 80.99	68.10 / 68.02%	56.14 / 55.96%	46.49 / 46.34%	37.39 / 37.32%
Novel (train/all data)	M	66.20 / 66.03%	%08.79 / 67.80%	64.94 / 64.80%	66.81 / 66.65%	64.23 / 64.08%	64.49 / 64.39%	54.52 / 54.40%	42.77 / 42.68%
	GPT	68.40 / 68.34%	72.37 / 72.26%	66.63 / 66.52%	71.50 / 71.40%	69.24 / 69.08%	63.02 / 62.83%	52.76 / 52.67%	33.85 / 33.77%
	M2	1.1485 ± 0.0045	1.1259 ± 0.0047	1.1277 ± 0.0045	1.0861 ± 0.0046	1.1449 ± 0.0044	1.1677 ± 0.0047	1.1389 ± 0.0049	1.0382 ± 0.0055
NP-Likeness	M	1.1403 ± 0.0046	1.1819 ± 0.0046	1.1592 ± 0.0046	1.1730 \pm 0.0045	1.1734 ± 0.0046	1.1095 ± 0.0045	1.1372 ± 0.0048	1.0667 ± 0.0053
	GPT	0.9960 ± 0.0047	1.0634 ± 0.0047	1.1595 ± 0.0047	1.0460 ± 0.0045	1.1655 ± 0.0045	1.1722 \pm 0.0047	1.0894 ± 0.0050	0.9399 ± 0.0057
	M2	4.1387 ± 0.0043	4.1309 ± 0.0044	4.0906 ± 0.0043	4.1219 ± 0.0045	4.1341 ± 0.0043	4.1753 ± 0.0044	4.1697 ± 0.0046	4.0715 ± 0.0055
SAScore	M	4.1673 ± 0.0043	4.1468 ± 0.0043	4.1568 ± 0.0043	4.2157 ± 0.0044	4.1980 ± 0.0045	4.1542 ± 0.0045	4.2129 ± 0.0048	4.1109 ± 0.0051
	GPT	4.1657 ± 0.0045	4.2461 ± 0.0044	4.3047 ± 0.0045	4.2467 ± 0.0044	4.2770 \pm 0.0042	4.2726 \pm 0.0044	4.1814 ± 0.0046	3.9353 ± 0.0053
F	M2	0.2187 sec	0.1217 sec	0.1805 sec	0.1384 sec	0.0442 sec	0.0208 sec	0.0167 sec	0.0053 sec
(per molecule)	M1	0.2302 sec	0.0801 sec	0.1745 sec	0.1394 sec	0.0455 sec	0.0110 sec	0.0045 sec	0.0070 sec
,,	GPT	0.1512 sec	0.0425 sec	0.1401 sec	0.0914 sec	0.0121 sec	0.0042 sec	0.0060 sec	0.0072 sec
Comit a citorion	M2	6 hr 4 min	3 hr 23 min	5 hr 2 min	3 hr 50 min	1 hr 13 min	34 min	27 min	8 min
deneration mine (total)	M1	6 hr 23 min	2 hr 13 min	4 hr 52 min	3 hr 52 min	1 hr 15 min	18 min	7 min	11 min
(:)	GPT	4 hr 12 min	1 hr 11 min	3 hr 55 min	2 hr 32 min	20 min	7 min	10 min	12 min
	M2	33199	30956	32072	35252	36688	28079	24884	21389
Unique Scaffolds	M1	33564	31505	32655	34844	32746	34947	30697	24067
	GPT	35237	34458	36523	38873	34945	30522	28936	17457
0	M2	24615	22104	24149	30675	31121	17993	14524	17663
Novel scalidis (v.s. training data)	M1	25619	23178	24849	26838	24396	29127	24918	18540
,	GPT	30607	27698	30717	33048	27555	20875	23954	13878
S S S S S S S S S S S S S S S S S S S	M2	22681	20156	22293	29029	29374	16464	13271	16856
(v.s. all data)	M1	23707	21204	22999	24963	22617	27547	23583	17509
(2000)	GPT	29015	25771	28933	31226	25685	19171	22747	13067

Figure 20: Molecule generation result table (scaffold split pre-trained models).

A

A.9 PSEUDO-NP ERROR ANALYSIS

Long-context modeling is not central to our tasks, as NP SMILES are relatively short (avg.<200 characters); instead, challenges arise from stereochemistry and structural diversity, which increase information density and complicate tokenization, particularly with rare or fused ring systems. To better understand these sources of difficulty in molecule generation, we perform error analysis using partialsmiles, a Python library that parses and validates partial SMILES strings by checking syntax, aromatic system kekulization, and atom valences against allowed ranges (O'Boyle, 2020). The parser reports three main types of errors: syntax errors (e.g., illegal characters, unmatched brackets, invalid SMILES structure, and more), valence errors (when an atom's valence is not on the allowed list for its charge state), and kekulization failures (when an aromatic system cannot be resolved into alternating bonds). These errors are raised as exceptions that can be caught programmatically, allowing for the diagnosis of why specific SMILES strings are invalid.

In Table 9, regarding tokenizers' average syntax error, NPBPEs with large vocabularies might have over-merged unrelated symbols that break chemical substructures, thus increasing the percentage of syntax errors. While BPE, NPBPE100, and 1000 seem to provide a more balanced trade-off in granularity and context and reduce the share of syntax errors, AIS still outperforms all tokenizers in validity, producing the highest number of valid molecules.

Furthermore, the error distribution aligns with the Pareto principle (Figure 21 and Table 10), with a few dominant error types (around 20%), such as kekulization failure, and unclosed ring openings, parentheses, and branches, accounting for the majority of failures (around 80%), pointing to key areas for targeted pesudo-NP molecules generation improvement.

Table 9: Model- and tokenizer-wise average error type.

Error Type		Char	BPE	AIS	NPBPE60	NPBPE100	NPBPE1000	NPBPE7924	NPBPE30k	Avg.
	Mamba-2	80.94%	80.00%	81.58%	78.98%	75.51%	80.59%	81.48%	87.72%	80.85%
Syntax	Mamba	77.07%	72.10%	77.47%	81.11%	73.85%	69.35%	85.22%	86.61%	77.85%
Error	GPT	79.30%	75.96%	81.02%	81.04%	80.68%	79.62%	85.34%	89.36%	81.54%
	Avg.	79.10%	76.02%	80.02%	80.38%	76.68%	76.52%	84.01%	87.90%	
	Mamba-2	12.39%	11.67%	13.32%	12.51%	16.42%	11.18%	12.46%	8.06%	12.25%
Kekulization	Mamba	16.18%	15.37%	17.52%	12.40%	16.79%	19.82%	8.93%	9.01%	14.50%
Failure	GPT	15.83%	14.49%	16.14%	14.57%	13.36%	13.42%	11.02%	7.83%	13.33%
	Avg.	14.80%	13.84%	15.66%	13.16%	15.52%	14.81%	10.80%	8.30%	
	Mamba-2	6.66%	8.33%	5.10%	8.49%	8.06%	8.23%	6.06%	4.22%	6.89%
Valence	Mamba	6.74%	12.52%	5.01%	6.48%	9.35%	10.83%	5.85%	4.38%	7.65%
Error	GPT	4.87%	9.56%	2.85%	4.39%	5.95%	6.96%	3.64%	2.81%	5.13%
	Avg.	6.09%	10.14%	4.32%	6.45%	7.79%	8.67%	5.18%	3.80%	

Table 10: Model- and tokenizer-wise averages for all error types.

Error Type	GPT	M1	M2	Char	BPE	AIS	NPBPE60	NPBPE100	NPBPE1000	NPBPE7924	NPBPE30k
Syntax: N ring openings have not been closed	48.32%	47.58%	44.76%	42.74%	46.72%	48.38%	44.85%	45.72%	48.70%	51.42%	46.60%
Syntax: Unmatched close parenthesis	14.82%	13.20%	18.18%	17.11%	11.75%	15.57%	13.90%	12.59%	11.26%	16.87%	24.18%
Kekulization: Aromatic system cannot be kekulized	13.33%	14.50%	12.25%	14.80%	13.84%	15.66%	13.16%	15.52%	14.81%	10.80%	8.30%
Syntax: N branches have not been closed	8.62%	4.30%	5.84%	5.33%	7.62%	7.41%	7.78%	5.56%	4.13%	5.57%	6.63%
Valence: Uncommon valence or charge state	5.13%	7.64%	%68.9	%60.9	10.14%	4.32%	6.45%	7.79%	8.67%	5.18%	3.80%
Syntax: Cannot have a second bond between the same atoms	4.39%	4.97%	4.56%	4.60%	3.77%	3.75%	4.00%	5.04%	5.52%	5.10%	5.34%
Syntax: Illegal character	1.34%	1.92%	1.73%	3.15%	1.65%	1.76%	3.60%	2.25%	0.60%	0.18%	0.12%
Syntax: Ring closure symbols must immediately follow an atom	1.01%	1.63%	1.44%	0.84%	0.34%	0.92%	1.17%	1.53%	2.52%	1.87%	1.67%
Syntax: Missing the close bracket	%99.0	0.92%	0.97%	1.81%	2.23%	0.00%	1.38%	0.86%	0.43%	0.06%	0.03%
Syntax: The final branch should not be within parentheses	0.39%	0.65%	0.62%	0.39%	0.19%	0.14%	0.38%	0.57%	%69.0	0.87%	1.19%
Syntax: An atom must precede an open parenthesis	0.39%	0.38%	0.44%	0.50%	0.21%	0.23%	0.48%	0.33%	0.58%	0.39%	0.54%
Syntax: Cannot have a bond opening and closing on the same	0.37%	0.59%	0.54%	0.67%	0.30%	0.61%	0.81%	0.68%	0.46%	0.26%	0.20%
atom											
Syntax: Only a single bond symbol should be used	0.33%	0.49%	0.49%	0.35%	0.33%	0.53%	0.45%	0.52%	0.56%	0.43%	0.35%
Syntax: Ring closure symbols should not be in parentheses	0.31%	0.46%	0.47%	0.50%	0.30%	0.41%	0.65%	0.37%	0.43%	0.35%	0.29%
Syntax: An atom must precede a bond symbol	0.17%	0.14%	0.14%	0.13%	0.04%	0.05%	0.12%	0.13%	0.17%	0.23%	0.34%
Syntax: Empty branches are not allowed	0.13%	0.20%	0.18%	0.31%	0.14%	0.11%	0.36%	0.13%	0.10%	0.12%	0.08%
Syntax: A bond symbol should not precede an open parenthesis	0.08%	0.12%	0.16%	0.12%	0.10%	0.08%	0.14%	0.16%	0.15%	0.12%	0.11%
Syntax: An atom must follow a bond symbol	0.06%	0.11%	0.13%	0.13%	0.08%	0.02%	0.15%	0.13%	0.11%	0.09%	0.09%
Syntax: An element symbol is required	0.06%	0.08%	0.10%	0.32%	0.09%	0.00%	0.10%	0.07%	0.05%	0.01%	0.01%
Syntax: An atom must precede a bond closure symbol	0.06%	0.07%	0.07%	0.04%	0.11%	0.06%	0.03%	0.03%	0.06%	0.06%	0.14%
Syntax: An open square brackets is present without the corresponding close square brackets	0.01%	0.02%	0.03%	0.06%	0.01%	0.00%	0.03%	0.02%	0.02%	0.00%	0.00%

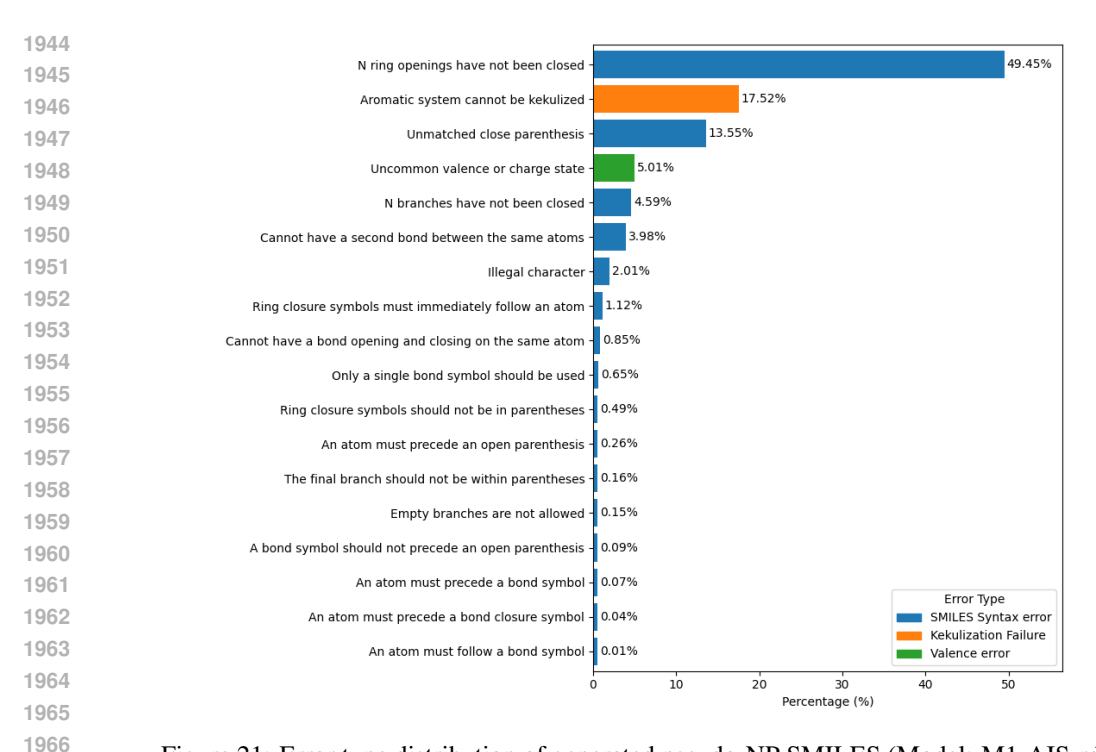


Figure 21: Error type distribution of generated pseudo-NP SMILES (Model: M1-AIS-rds).

A.10 SCAFFOLDS

 Scaffolds are the core frameworks of molecules, and they are essential for classifying compounds and predicting biological activity (Bemis & Murcko, 1996). Thus, their investigation facilitates the identification of privileged substructures and provides insights that are essential for drug development (Hu et al., 2016; 2011; Sato et al., 2021). The scaffold distribution in the 1M NP dataset follows Zipf's law precisely (see Figure 22), meaning the most frequent scaffold appears approximately twice as often as the second most frequent, three times as often as the third, and so forth. A visualization of the most commonly occurring scaffolds in 1M NPs is provided in Figure 24.

As shown in Table 2 in the main text, tokenizers with more fine-grained tokens, like Character-level and NPBPE60, appear to perform better when generating novel scaffolds, contrasting with the earlier observation that the atom-level AIS tokenizer is more effective for generating entire molecules. Scaffolds perhaps benefit from finer-grained tokenization because they involve core substructures that recur with subtle variations, and fine-grained tokens offer such flexibility; however, a better understanding of what underlies this phenomenon might require more chemical and domain-specific expertise.

Regarding scaffold diversity within each model-tokenizer pair's generated molecules, we can observe that they are able to mimic the scaffold diversity present in the training data very well, as they closely resemble the 1M NP's scaffold Zipfian distribution (see Figure 22). The total number of unique and novel scaffolds also suggests that all novel scaffolds lie in the long tail of the Zipfian distributions since these novel scaffolds appear fewer than 10 times each in every model-generated dataset, as shown in Figures 25 and 26.

In addition, Figure 23 shows low pairwise Jaccard similarity values (0.05 to 0.11) between each two sets of scaffolds, suggesting that different models are exploring fairly distinct chemical spaces. Notably, NPBPE30k appears more distinct from other tokenizers while not exhibiting high overlap with the training data, possibly due to its already generating fewer unique scaffolds in the first place.

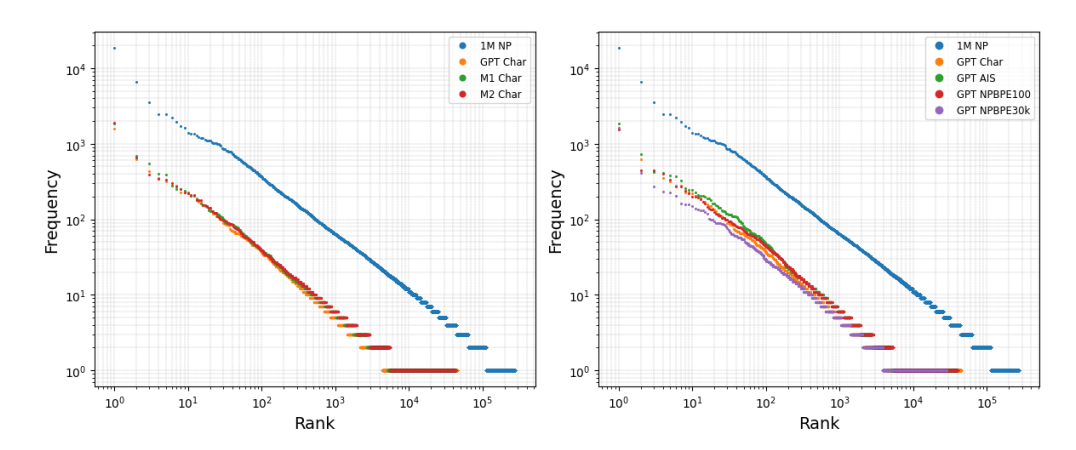


Figure 22: **Zipf's law in scaffold rank-frequency distributions across datasets,** the log-log rank-frequency distributions of all scaffolds of the generated molecules (generated by selected random split pre-trained models) vs. the 1M NP dataset; the x-axis denotes the rank of each unique scaffold based on its occurrence, while the y-axis represents its frequency.

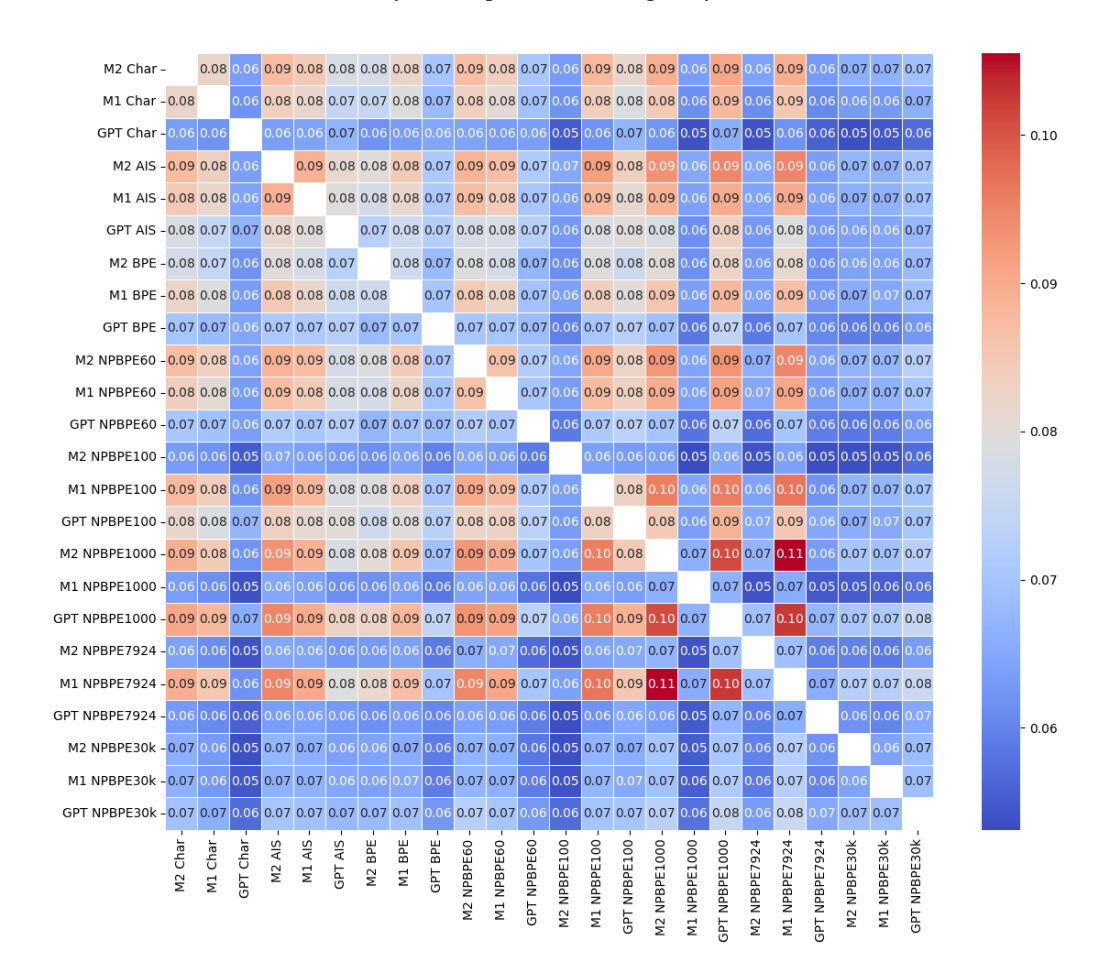


Figure 23: **Jaccard similarity heatmap of scaffold sets.** The heatmap visualizes the pairwise Jaccard similarity between scaffold sets (without duplicates, generated by random split pre-trained models); diagonal self-similarity values are excluded; the color scale represents the similarity values, with warmer colors indicating higher similarity; since the unique scaffold counts for each set range from approximately 30,000 to 45,000, a difference of 0.01 in Jaccard similarity corresponds to an overlap of approximately 550 to 850 scaffolds.

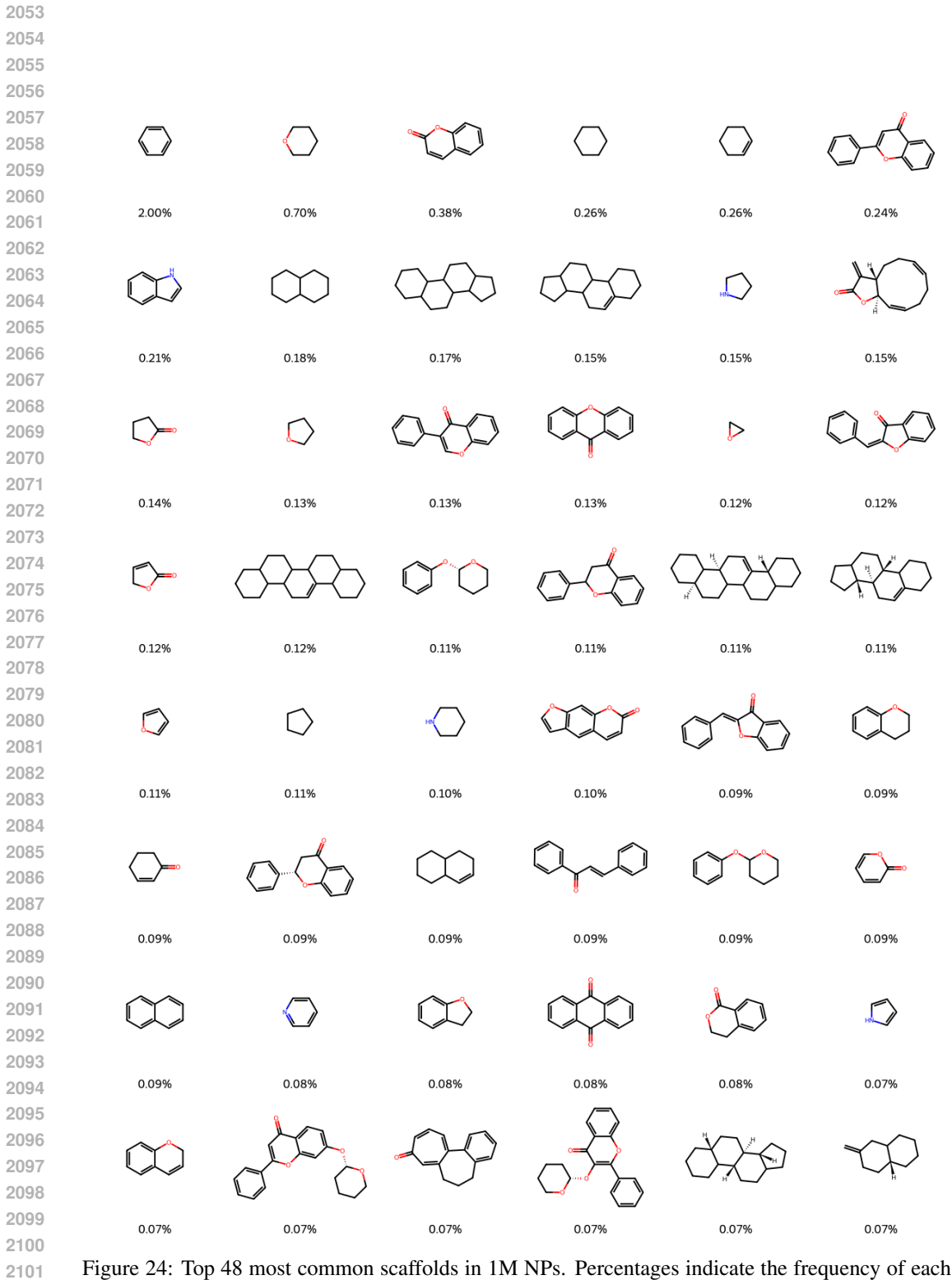


Figure 24: Top 48 most common scaffolds in 1M NPs. Percentages indicate the frequency of each scaffold's occurrence.

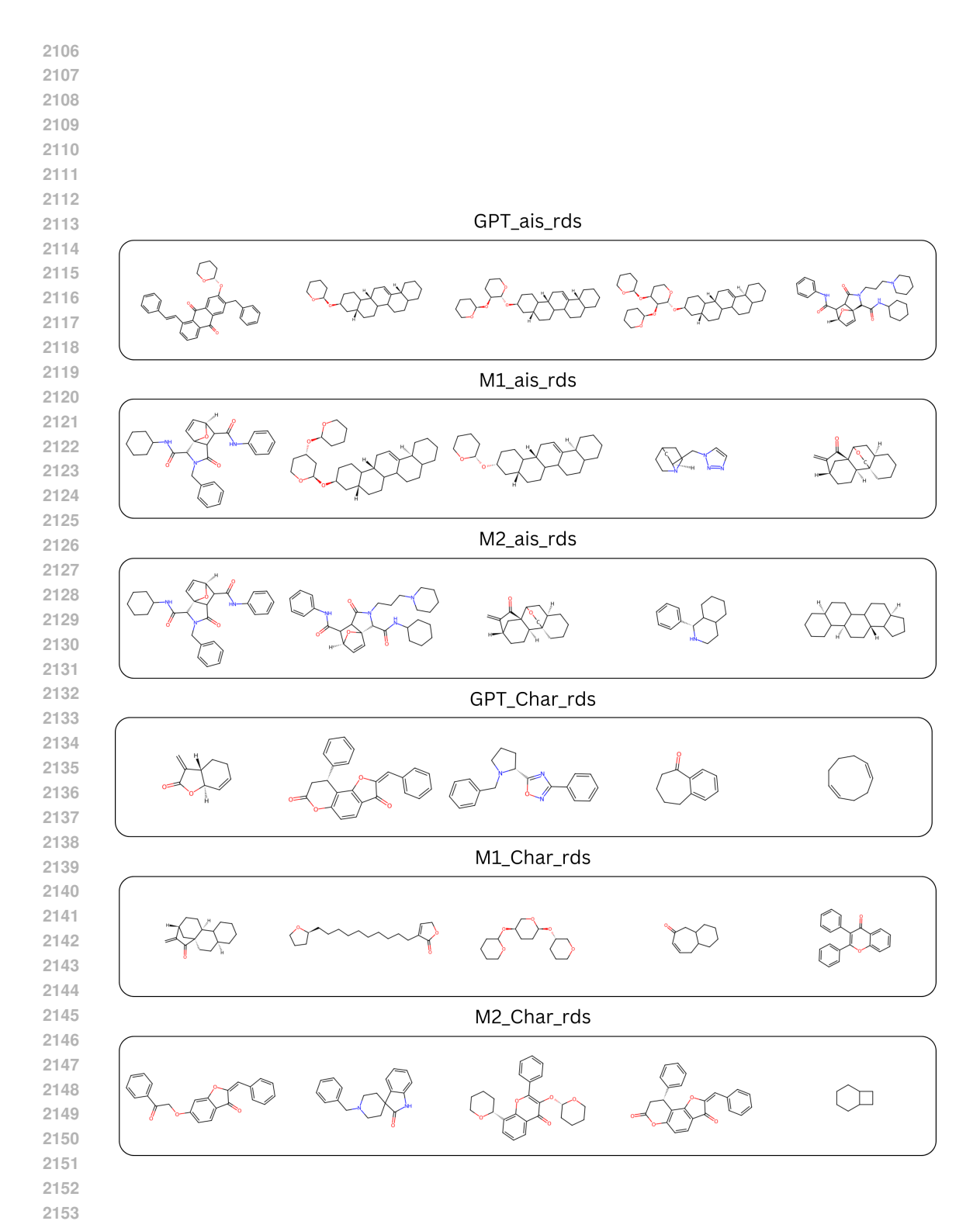


Figure 25: Top 5 most frequently occurring novel scaffolds from molecules generated by selected models - part 1 (with frequencies around 0.01%-0.02%).

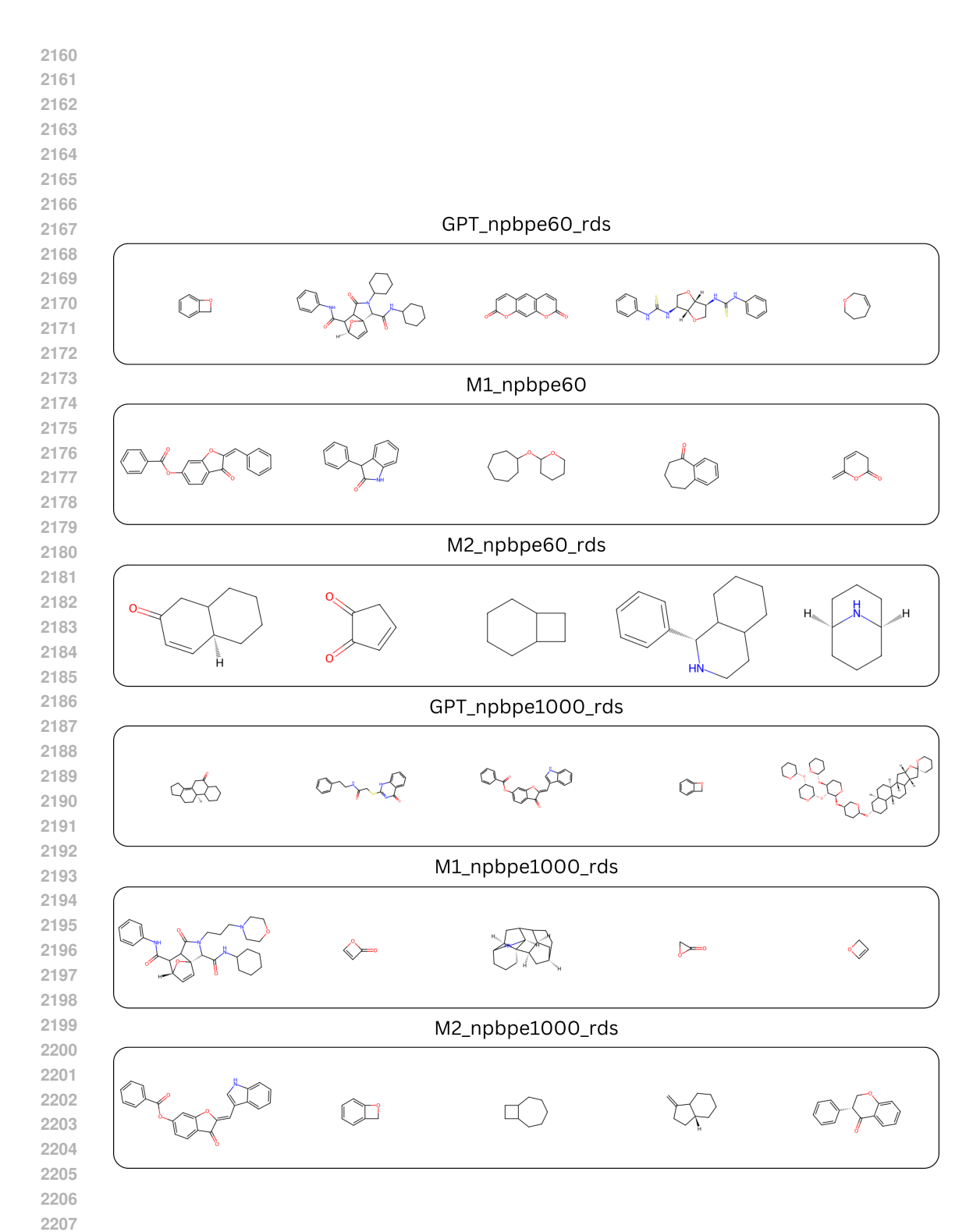


Figure 26: Top 5 most frequently occurring novel scaffolds from molecules generated by selected models - part 2 (with frequencies around 0.01%-0.02%).

A.11 SYNTHETIC ACCESSIBILITY & NP-LIKENESS

The NP-likeness score and SAScore are widely used cheminformatics metrics developed over a decade ago to evaluate NP similarity and molecule synthetic accessibility. NP-likeness score, developed in 2008 by Ertl et al. (2008), is a naive Bayesian-based measure designed to evaluate how structurally similar a given molecule is to known NPs. It has been trained on approximately 115,000 NPs and nearly 300,000 synthetic molecules from commercial libraries, assigning fragment-based scores that reflect structural similarity to known NPs. The score can range from -5 to 5, with higher values indicating greater structural similarity to NPs. Synthetic accessibility score (SAScore), developed by Ertl & Schuffenhauer (2009), assesses the ease of synthesizing drug-like molecules by combining fragment frequency (from PubChem) with penalties for structural complexity, outputting a score from 1 (easy) to 10 (hard). While both metrics are fast and interpretable, they rely on potentially outdated fragment libraries and limited validation, risking poor generalization to novel NPs or synthetically tractable but complex molecules. For completeness, we report both metrics in Table 11, and in Figures 19 and 20; however, we ultimately consider them limited and outdated for the robust evaluation of machine-generated pseudo-NPs that have learned from the more modern NP compound libraries.

Several retrosynthesis tools, such as AiZynthFinder, Chemformer, IBM RXN, Merck Synthia, and ASKCOS, offer automated synthesis route planning and have been successfully applied to a wide range of small synthetic molecules. However, these models are ultimately not designed for NPs, which have more structural complexity. For completeness, we have applied ASKCOS¹⁹ to 25 de novo generated pseudo-NP SMILES strings and reported four resulting retrosynthesis trees (Figure 27) (Tu et al., 2025). In most cases, the model failed to identify valid synthetic routes, highlighting limited applicability to novel NP-like scaffolds. When routes can be found, they are generally plausible; however, many precursor compounds received strongly negative scores, suggesting they are rare, costly, or synthetically impractical.

While synthetic accessibility is an important consideration in drug discovery, it is ultimately not the primary focus of this work. NPs themselves are often synthetically challenging, and this complexity can only increase in machine-generated pseudo-NPs that explore new regions of chemical space. This work centers on evaluating state-space models and tokenizer combinations for NPCLMs. A thorough assessment of synthetic accessibility for pseudo-NPs will be pursued in future work.

Table 11: **Tokenizer- and model-wise averaged NP-likeness and SAScore**: combining both scaffold and random split pre-trained model generation results.

	NP-likeness	SAScore
1M NP Avg.	1.23	4.47
Tokenizer-wise Avg.		
Character-level	1.09	4.20
AIS	1.11	4.20
BPE	1.10	4.19
NPBPE60	1.08	4.22
NPBPE100	1.14	4.25
NPBPE1000	1.13	4.25
NPBPE7924	1.08	4.20
NPBPE30k	1.00	4.10
Model-wise Avg.		
Mamba-2	1.11	4.18
Mamba	1.12	4.21
GPT	1.05	4.21

¹⁹https://askcos.mit.edu/

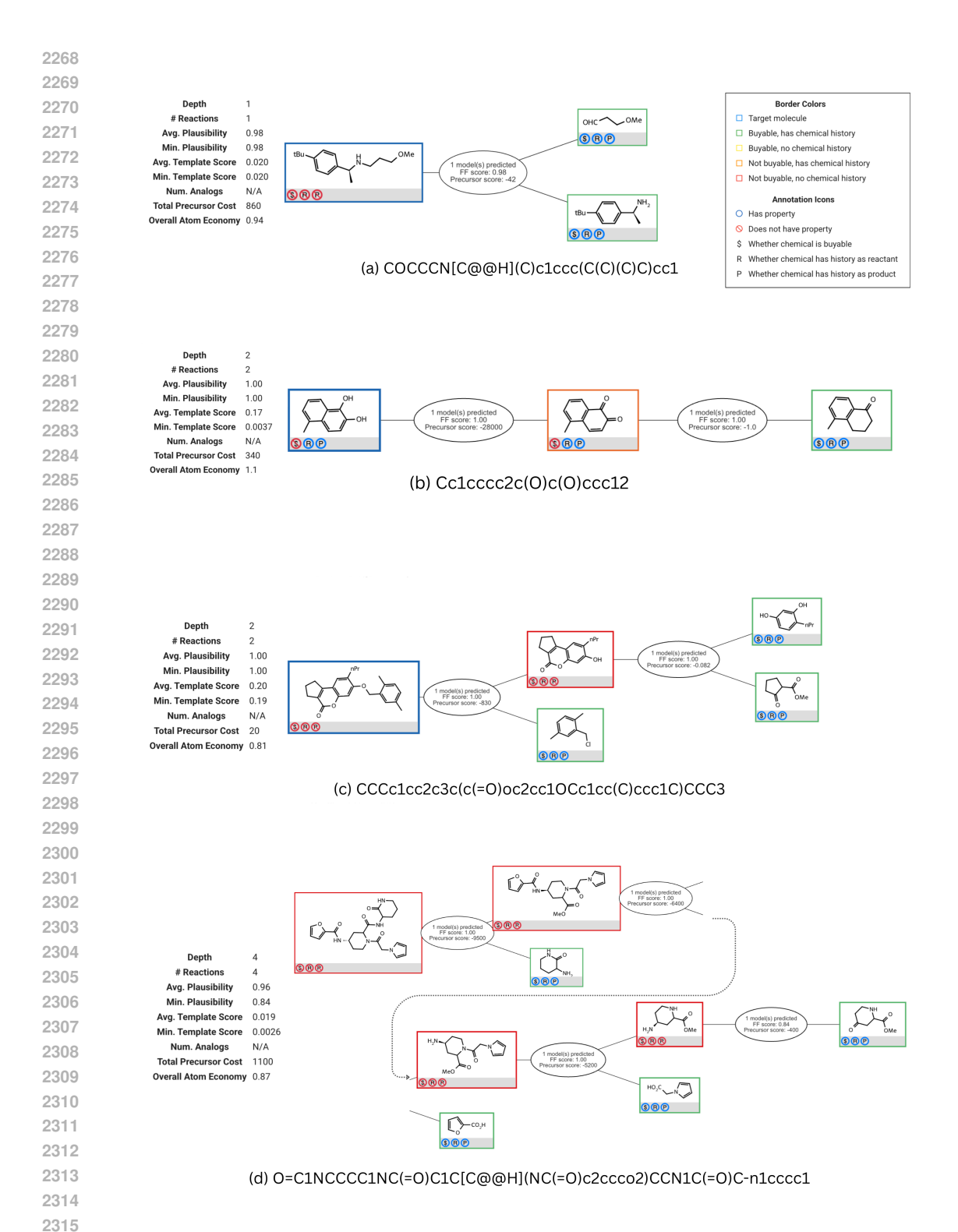


Figure 27: Retrosynthetic pathway analyses of representative pseudo-NP molecules generated by the M1-ais-rds model. Retrosynthetic trees were constructed using ASKCOS (backend: template_relevance; tree builder: MCTS).

A.12 PRE-TRAINING DETAILS

Before training begins, 5% of the training and validation data is used for a random search that explores half of all possible combinations for the best hyperparameters for each model and tokenizer pair. The hyperparameter search space is shown in Table 12. There are 48 model variations, consisting of 24 model-tokenizer pairs (3 model types times 8 tokenizers) across two data-splitting strategies: scaffold split and random split. Tokenized SMILES sequences are truncated or padded to a fixed length of 512 tokens for batch processing, and cross-entropy loss is used as the objective function. After the hyperparameter search is completed, each model is initialized with its optimal hyperparameters and trained until convergence. The maximum number of training epochs for each model is 150, and training stops if the validation loss does not improve for 5 subsequent epochs. All models in this study have converged before reaching 150 epochs. After training, the final evaluation is performed on the test set that has not been seen by the models during training. A100 GPUs are used for all training processes, and the total training time taken for each model to converge ranges from a few hours to around a week. Figures 28, 29, and 30 show the pre-training details for each model and tokenizer combination in this study.

Sharpness Aware Minimization (SAM) is used as an optimization strategy during training to improve model generalization (Foret et al., 2020). The code implementation in this work is adapted from the work of Tsai et al. (2024) in their open source repository²⁰. SAM can improve model generalization by simultaneously minimizing both the value of the loss function and the sharpness of the loss landscape. It is motivated by the idea that flatter minima in the loss landscape lead to better generalization in overparameterized models. Rather than only focusing on a low-loss parameter configuration, SAM seeks parameter regions where the loss remains low across a neighborhood. Implementing SAM requires calculating the loss and performing backpropagation twice per iteration—first to estimate an adversarial perturbation and then to compute the final gradient—which doubles the computational cost compared to standard methods.

Table 12: Pre-training hyperparameter search space.

Hyperparameters	Mamba and Mamba-2	GPT
Number of Mamba Blocks	4, 8, 12	n.a.
Number of Transformer Blocks	n.a.	4, 8, 12
Number of Attention Heads	n.a.	2, 4, 8
Embedding Size	256, 51	12
MLP/FF dimension	Embedding S	Size * 4
Learning Rate	1e-3, 5e-3, 1e	e-4, 5e-4
Batch Size	32	
SAM - L2 Weight Decay	1e-4	
SAM - Perturbation Radius (ρ)	0.05	

²⁰https://github.com/tiffany9056/UU-Mamba.git

2376				ı							
2377	30k)	şţş	8	Loss: 5.6934 Perplexity: 296.9032	2		sb	8	905	۔ ج	
2378	NPBPE30k (vocab_size = 30k)	M2-npbpe30k-sfs 50.2M	d_model: 512 n_layer: 4 lr: 0.001	Loss: 5.6934 olexity: 296.9	18hr 15min (30min/epoch)	_	M2-npbpe30k-rds 69.7M	d_model: 512 n_layer: 8 lr: 0.0005	Loss: 3.6911 Perplexity: 40.0905	1d 10hr 1min (39min/epoch)	.⊑
2379	BPE siz	obpe30 50.2M	_model: 51 n_layer: 4 lr: 0.001	s: 5.	hr 15 nin/e	8min	obpe30 69.7M	laye 0.00	s: 3. xity:	10hr Jin/e	15min
2380	Sab P	2-np	בׁן ב' <u>=</u>	Los	18 (30n		2-np	유 c' 등	Los	1d (39n	
2381		Σ		Pe			Σ		P		
2382	924)	sts	01	200	_		rds	01	305	_	
2383	7924 = 7	924	. 512 . 12 01	3402 38.10	min	_	924-	: 512 r: 8 05	7081 15.0(min Soch	_
2384	NPBPE7924	M2-npbpe7924-sfs 66.5M	d_model: 512 n_layer: 12 lr: 0.0001	Loss: 3.6402 Perplexity: 38.1004	1d 3hr 5min (55min/epoch)	27min	M2-npbpe7924-rds 47M	d_model: 512 n_layer: 8 lr: 0.0005	Loss: 2.7081 Perplexity: 15.0005	21hr 15min (40min/epoch)	23min
2385	Sab a	dr.	티디브	Los	1d (.,	현	و ^{ا د} ا ب	Los	21k (40m	.,
2386	٤	MZ		Pe			M		Pe		
2387	000	sfs		322			ş		29		
2388	NPBPE1000 :ab_size = 10	M2-npbpe1000-sfs 59.4M	d_model: 512 n_layer: 12 lr: 0.0001	Loss: 2.3314 Perplexity: 10.2922	23hr 30min (1hr10/epoch)	_	M2-npbpe1000-rds 59.4M	d_model: 512 n_layer: 12 lr: 0.0001	Loss: 1.3155 Perplexity: 3.7267	3d 4hr 35min (1hr/epoch)	_
2389	3PE1	bpe100 59.4M	_model: 51; n_layer: 12 lr: 0.0001	s: 2.3	23hr 30min Ihr10/epoch	34min	bpe10 59.4M	odel ayer 0.00	s: 1.8 xity:	d 4hr 35mir (1hr/epoch)	45min
2390	N PE	dd- 5	ا ا	Loss	23r 11r1	(+)	ddr.	ا دا ا	Loss	3d 4 (1h)	4
2391	Š	M2		Pe			MZ		P		
2392	NPBPE100 NPBPE1000 NPBPE7924 (vocab_size = 100) (vocab_size = 100) (vocab_size = 7924)	şį.		82			ş		36		
2393	100	M2-npbpe100-sfs 58.5M	d_model: 512 n_layer: 12 lr: 0.0005	Loss: 1.2084 Perplexity: 3.3482	1d 9hr 5min (1hr20/epoch)	Ξ	M2-npbpe100-rds 39M	d_model: 512 n_layer: 8 lr: 0.0005	Loss: 0.8388 Perplexity: 2.3136	1d 23hr 17min (50min/epoch)	듣
2394	NPBPE100	bpe10 58.5M	_model: 512 n_layer: 12 lr: 0.0005	:: 1.2	1d 9hr 5min 1hr20/epoch	1hr 13min	bpe1 39M	_model: 512 n_layer: 8 lr: 0.0005	:: 0.8 dity:::	3hr 1 in/ep	1hr 15min
2395	Sa P.	inp!		Loss: 1.2084 erplexity: 3.34	1d 9	Ę	dr.	ق <u>- ا ::</u>	Loss	d 23 50m	투
2396	٤	MZ	Ū	Pe			M	Ū	Pe		
2397	6	က္က		4			<u>s</u>		11	_	
2398	NPBPE60 (vocab_size = 60)	M2-npbpe60-sfs 58.5M	d_model: 512 n_layer: 12 lr: 0.0005	Loss: 0.7558 Perplexity: 2.1294	2d 9hr 4min (1hr50/epoch)	·Ę	M2-npbpe60-rds 58.5M	d_model: 512 n_layer: 12 lr: 0.0001	Loss: 0.3837 Perplexity: 1.4677	4d 17hr 20min (2hr11/epoch)	.⊑
2399	NPBPE60	obpe6 58.5M	_model: 51; n_layer: 12 lr: 0.0005	Loss: 0.7558 rplexity: 2.129	2d 9hr 4min 1hr50/epoch	3hr 50min	pbpe6 58.5M	_model: 51: n_layer: 12 lr: 0.0001	Loss: 0.3837 erplexity: 1.46	'hr 2 1/ep	4hr 16min
2400	NP Cab	2-np 5	E 5 5	Loss	2d 9 1hr5	3hr	2-np 5	E 2 2	Loss	d 17 2hr1	4h
2401 2402	٤	Σ̈́	J	Pe			ž	J	Pe	4 ~	
2402	24)			98	<u> </u>				22		
2404	= 79	sts	512 12 11	Loss: 0.7123 Perplexity: 2.0386	3d 17hr (2hr15min/epoch)	_	ş	512 4 11	Loss: 0.4089 Perplexity: 1.5052	고 등	.⊑
2405	BPE	-BPE-s 66.5M	_model: 512 n_layer: 12 lr: 0.0001	: 0.7	3d 17hr 5min/epc	5hr 2min	-BPE-r 27.6M	_model: 51 n_layer: 4 lr: 0.0001	: 0.4 ity: 1	4d 21hr (1hr/epoch)	1hr 59min
2406	ab_s	M2-BPE-sfs 66.5M	d_model: 512 n_layer: 12 lr: 0.0001	Loss: 0.7123	3 115	5hı	M2-BPE-rds 27.6M	d_model: 512 n_layer: 4 lr: 0.0001	Loss: 0.4089 erplexity: 1.50	(1hr	후
2407	, V		O	Pe l	2			0	Pe		
	s 23)			80					Σ	_ _	
2409	19 19	sts	512 12)1	210 .860	nin och)	.⊑	şp_	512 12)1	479 .416	2min poct	ے.
2410	n-SI size	M2-AIS-sfs 59.4M	_model: 51; n_layer: 12 lr: 0.0001	: 0.6 ity: 1	2d 6hr 5min 2hr50/epoch	3hr 23min	M2-AIS-rds 59.4M	_model: 512 n_layer: 12 lr: 0.0001	: 0.3 ity: 1	hr 1; nin/e	4hr 9min
2411	Atom-in-SMILES rocab_size = 1023	M2-/	d_model: 512 n_layer: 12 lr: 0.0001	Loss: 0.6210 Perplexity: 1.8608	2d 6hr 5min (2hr50/epoch)	3hr	M2-/	d_model: 512 n_layer: 12 lr: 0.0001	Loss: 0.3479 Perplexity: 1.4161	4d 18hr 12min (2hr15min/epoch)	4
2412	Atom-in-SMILES BPE (vocab_size = 1924)		O	Pe L	3			0	Pe L	4 7	
2413	_			œ	<u>-</u>				œ	<u>-</u>	
2414	Character-Level (vocab_size = 48)	-sts	512 12)1	Loss: 0.5335 Perplexity: 1.7048	6d 18hr 13min (2hr50min/epoch)	.⊑	rds	512 12 11	Loss: 0.2977 Perplexity: 1.3468	8d 8hr 11min (2hr50min/epoch)	.⊑
2415	size	M2-Char-sfs 58.4M	d_model: 512 n_layer: 12 lr: 0.0001	Loss: 0.5335 erplexity: 1.70	6d 18hr 13min 2hr50min/epoch	6hr 4min	M2-Char-rds 58.4M	d_model: 512 n_layer: 12 lr: 0.0001	Loss: 0.2977 erplexity: 1.34	8d 8hr 11min hr50min/epoc	7hr 39min
2416	arac cab_	M2-C	_mo n_la lr: 0	oss.	d 18 Ir50n	6hr	42-C	n n n	oss.	3d 8F	7hr
2417	င် §	_	О	Pel L	9 42			0	Pel L	8 2	
2418			ည		_	m		SLS	_		6
2419	Model Details	ıme/	Best Hyper-Parameters	Test Loss and Perplexity	Training Time	Inference Time (10k Molecule Generation)	ıme/	Best Hyper-Parameters	Test Loss and Perplexity	Training Time	Inference Time (10k Molecule Generation)
2420	e l	Model Name/ Size	Best Parar	st Loss an Perplexity	ing	ference Tirr (10k Molecule Generation)	Model Name/ Size	Best -Paran	st Loss ar Perplexity	ing	ference Tirr (10k Molecule Generation)
2421	lode	l gol	F Jer-F	est I Per	rain	ifere (10k Gen	Mode	F. Jer-F	est I Per	rain	(10k Gen
2422	2		Ę	F	-	드		Ą	-	_	드
2423	μ			t Se					E J		
2424 2425	Data Split			Scaffold Split					Random Split		
2425	Da			Ñ					άž		
2427	<u> </u>					ba					
2428	Model					Mamba	7				
2429	-					2					
							_	_			

Figure 28: Mamba-2 training details.

0.400											
2430	용	sts		134			sp.		159		
2431	NPBPE30k (vocab_size = 30k)	M1-npbpe30k-sfs 69.5M	d_model: 512 n_layer: 8 lr: 0.0005	Loss: 5.3646 Perplexity: 213.7134	14hr 7min (25min/epoch)	_	M1-npbpe30k-rds 69.5M	d_model: 512 n_layer: 8 lr: 0.0005	Loss: 3.6825 Perplexity: 39.7459	1d 1hr 5min (30min/epoch)	_
2432	NPBPE30k ab_size = 3	bpe30 69.5M	_model: 51 n_layer: 8 lr: 0.0005	s: 5.3 ty: 2	14hr 7min 5min/epoc	11min	bpe30 69.5M	_model: 51 n_layer: 8 lr: 0.0005	3: 3.6 ity: 3	1d 1hr 5min 30min/epoch	10min
2433 2434	₽ å	du- 9	트 리브	Loss	14I 25m	_	후	ج اے ا	Loss Plex	1d ,	_
2435	ક્	Z		Per			Σ		Per		
2436	24	şĮş		10			န		7		
	324 = 79	24-8	256 4 15	768 3.27	in och)		24-r	521 8 11	349	min och)	
2437 2438	PE79	bpe79 8.96M	del:	3.8 Y: 4	8hr 27min 2min/epocl	7min	bpe79; 46.9M	_model: 52 n_layer: 8 lr: 0.0001	2.0; ity: 7	r 14 γeρ	14min
2439	NPBPE7924 :ab_size = 79	npb 8.	d_model: 256 n_layer: 4 lr: 0.0005	Loss: 3.8768 Perplexity: 48.2701	8hr 27min (12min/epoch)	_	ddr 4	d_model: 521 n_layer: 8 lr: 0.0001	Loss: 2.0349 Perplexity: 7.6517	2d 4hr 14min (30min/epoch)	7
2440	- 8	M1-npbpe7924-sfs 8.96M	ъ	Per	Ξ		M1-npbpe7924-rds 46.9M	ъ	Per L	(4 (9)	
2441	6			22					00		
2442	9 =	s-00	512 8 5	116 080	r (g		5	512 8 5	Loss: 1.7016 Perplexity: 5.4828	ie G	
2443	NPBPE1000 :ab_size = 10	bpe10 39.8M	d_model: 512 n_layer: 8 lr: 0.0005	Loss: 2.4916 rplexity: 12.08	11hr 30min (30min/epoch)	18min	bpe100 39.8M	d_model: 512 n_layer: 8 lr: 0.0005	Loss: 1.7016 erplexity: 5.482	1d 1hr 48min (37min/epoch)	23min
2444	PP S	gddi 39	n n n n n n n n n n n n n n n n n n n	oss: lexit	11hr Omin	18	9b 39	_mor_ n_la lr: 0.	oss: olexif	d thi	23
2445	(vocab_size = 1000) (vocab_size = 7924)	M1-npbpe1000-sfs 39.8M	ס'	Loss: 2.4916 Perplexity: 12.0805	, ©		M1-npbpe1000-rds 39.8M	ס'	Per	3 7	
2446											
2447	NPBPE100 (vocab_size = 100)	M1-npbpe100-sfs 58.2M	212 1	Loss: 1.1526 Perplexity: 3.1663	.⊑ ਰਿੰ	_	M1-npbpe100-rds 58.2M	212 1	Loss: 0.6500 Perplexity: 1.9156	흔운	_
2448	NPBPE100 :ab_size = 1	bpe10 58.2M	d_model: 512 n_layer: 12 lr: 0.0001	Loss: 1.1526 erplexity: 3.16	15hr 20min (1hr15/epoch)	1hr 15min	bpe10 58.2M	d_model: 512 n_layer: 12 lr: 0.0001	Loss: 0.6500 erplexity: 1.91	6d 21hr 46min (1hr10/epoch)	1hr 27min
2449	PB de	pbp 58.	_moc _lay lr: 0.	oss: olexit	5hr hr15	Thr 1	95 58	_moc lay lr: 0.	oss:	21h hr10	1hr
2450	Z 000	M1-	ام ام	Lo	- €		Ā	م' ت	Perp	9 E	
2451											
2452	NPBPE60 (vocab_size = 60)	M1-npbpe60-sfs 58.2M	2 12	Loss: 0.6920 Perplexity: 1.9978	들융	_	M1-npbpe60-rds 9.83M	3 56	Loss: 0.3959 Perplexity: 1.4856	ii (f	_
2453	NPBPE60 ab_size =	pbpe60 58.2M	d_model: 512 n_layer: 12 lr: 0.0001	Loss: 0.6920 erplexity: 1.997	2d 4hr 26min (2hr50/epoch)	3hr 52min	pbpe60 9.83M	d_model: 256 n_layer: 8 lr: 0.0001	Loss: 0.3959 erplexity: 1.48	1d 21hr 9min (34min/epoch)	1hr 20min
2454	ab s	npb _l 58.	mod lay	oss: (14hr 1750/	3hr 5	ddn 8.6	mod r: 0.	oss: (121 Imin	1hr 2
2455	_ š	M1-	ع اه	Lo	2 5	.,	Ę	۵' -	Perp	5 %	,
2456											
2457	792	<u>s</u>	2 2	38 356	٦ ((_	<u>s</u>	2 2	13	och)	_
2458	BPE size =	E-sí 2M	el: 5 er: 1; 0001).71(/: 2.(- 5mi	2mir	-BPE-rc 66.2M	el: 5 er: 1; 0001	.1.4	-44n	7mir
2459	B S	M1-BPE-sfs 66.2M	d_model: 512 n_layer: 12 lr: 0.0001	Loss: 0.7108 rplexity: 2.03	4d 3hr 5min (2hr35/epoch)	4hr 52min	M1-BPE-rds 66.2M	d_model: 512 n_layer: 12 lr: 0.0001	Loss: 0.4013 erplexity: 1.490	7d 13hr 44min (2hr50min/epoch)	5hr 17min
2460	Atom-in-SMILES BPE vocab_size = 7924)	Σ	م ام	Loss: 0.7108 Perplexity: 2.0356	4 (2)	1	Σ	اء ا	Loss: 0.4013 Perplexity: 1.4937	7d (2hr	4,
2461	⊛ ≥										
2462	LES 102	s	12	Loss: 0.6288 Perplexity: 1.8754	j= £	_	ø	2 2	Loss: 0.3552 Perplexity: 1.4265	. <u>Е</u> _	
2463 2464	SMI Se =	M1-AIS-sfs 39.8M	d_model: 512 n_layer: 8 lr: 0.0001	Loss: 0.6288 erplexity: 1.87	1d 23hr 25min (1hr40/epoch)	2hr 13min	M1-AIS-rds 59.1M	d_model: 512 n_layer: 12 lr: 0.0001	Loss: 0.3552 erplexity: 1.42	7d 9hr 24min (2hr10min)	3h 29min
2465	n-is	11-AI	mod lay	ss: (lexit	23hr 1r40/	hr 1	1-AIS-r 59.1M	mod lay	ss: (lexit	9hr 2hr1	3h 29
2466	Atom-in-SMILES /ocab_size = 102	2	۵, ۲ _	Lo Perp	₽ <u></u>	· · ·	Σ	ے او	Perp	р :S	,,
2467	٤.								_		
2468	Character-Level (vocab_size = 48)	હ	2 2	Loss: 0.5317 Perplexity: 1.7018	in Och)	_	ş	12	Loss: 0.3041 Perplexity: 1.3554	ir Sch)	
2469	Character-Level	M1-Char-sfs 58.1M	d_model: 512 n_layer: 12 lr: 0.0001	Loss: 0.5317 erplexity: 1.70	4d 17hr 9min hr45min/epoc	6hr 23min	M1-Char-rds 38.8M	d_model: 512 n_layer: 8 lr: 0.0001	Loss: 0.3041 erplexity: 1.35	7d 12hr 10min 2hr10min/epoch	<u> </u>
2470	ract b_s	I-Char-∉ 58.1M	mod laye	ss: (lexity	17h I5mi	hr 2	-Char- 38.8M	mod lay	ss: (lexity	12hr Omi	5hr
2471	Cha	Ě	- '- '명	Lo Perp	4d 17hr 9min (2hr45min/epoch)	9	Σ	9	Lo Perp	7d 12hr 10min (2hr10min/epoch)	
2472	_			_	_				_		
2473	<u>:</u>)e	eters	ը _	В	в 。_	<u>)</u>	eters	ը _	ng	e a
2474	Deta	Nam	st	ss a exity	I Traini Time	ce Ti olecul ation)	Nam	st	ss a exity	aini B	se Ti
2475	Model Details	Model Name/ Size	Best r-Parar	Test Loss and Perplexity	Total Training Time	Inference Time (10k Molecule Generation)	Model Name/ Size	Best r-Paran	Test Loss and Perplexity	Total Training Time	Inference Time (10k Molecule Generation)
2476	ĕ	Ĭ	Best Hyper-Parameters	를 라	Ď	interior in the second	Ĭ	Best Hyper-Parameters	Ţēs P	Į,	Infe
2477	±			-				_	:		
2478	Data Split			Scaffold Split					Random Split		
2479	Data			Sca					Ran Sı		
2480						æ	I				
2481	Model					Mamba 1					
2482	ž					Σ					
2483											

Figure 29: Mamba training details.

2484 2485	NPBPE100 NPBPE1000 NPBPE7924 NPBPE30k (vocab_size = 100) (vocab_size = 30k)	GPT-npbpe30k-sfs 56.2M	512 8 8 1	Loss: 5.8333 Perplexity: 341.4829	in och)		GPT-npbpe100-rds GPT-npbpe1000-rds GPT-npbpe30k-rds 13.0M 13.9M 21M 21M 43.6M	512 4 8 5	Loss: 3.8917 Perplexity: 48.9935	ch)	
2486	NPBPE30k :ab_size = 3	pbpe3 56.2M	n_embd: 512 n_layer: 8 n_head: 8 lr: 0.001	Loss: 5.8333 plexity: 341.4	5hr 27min (16min/epoch)	12min	pbpe3(43.6M	n_embd: 512 n_layer: 4 n_head: 8 lr: 0.0005	Loss: 3.8917 rplexity: 48.99	11hr (11min/epoch)	9min
2487	NPB	-inpl		oss.	5hr 16mi	7	Ā.		oss	1 E	0
2488 2489	, Vo	GP	_	Perp	٠		G	_	Per	٠	
2489	24)	sts		87			ş		24		
2491	924 = 79	924-	512 4 8 35	Loss: 4.0420 Perplexity: 56.9387	i (ch	_	924-	512 4 8 5	Loss: 2.9623 Perplexity: 19.3424	n (hoo	
2492	PE7	bpe7 21M	_embd: 51 n_layer: 4 n_head: 8 lr: 0.0005	: 4.0 ty: 5	6hr 11min min/epoch	10min	bpe7 21M	_embd: 51. n_layer: 4 n_head: 8 lr: 0.0005	: 2.9 ty: 1	6hr 1min)min/epoc	16min
2493	NPBPE7924 :ab_size = 79	du.'	n_embd: 512 n_layer: 4 n_head: 8 lr: 0.0005	Loss: 4.0420 rplexity: 56.93	6hr 11min (9min/epoch)	-	dr.,	n_embd: 512 n_layer: 4 n_head: 8 lr: 0.0005	Loss: 2.9623 rplexity: 19.34	6hr 1min (10min/epoch)	-
2494		GPT-npbpe1000-sfs GPT-npbpe7924-sfs 13.9M 21M	_	Per	Ŭ		GPT	_	Per L	٠	
2495	(00	sts		26			ş		23		
2496	000 = 10	é _	512 4 1.8 11	Loss: 2.3754 Perplexity: 10.7556	nin och)		<u>-</u>	512 4 1.8	Loss: 1.4130 Perplexity: 4.1083	ri (ho	
2497	NPBPE1000 :ab_size = 10	13.9M	n_embd: 512 n_layer: 4 n_head: 8 lr: 0.0001	Loss: 2.3754 rplexity: 10.75	7hr 22min (10min/epoch)	7min	obpe10 13.9M	n_embd: 512 n_layer: 4 n_head: 8 lr: 0.0001	Loss: 1.4130 erplexity: 4.10	20hr 3min (11min/epoch)	8min
2498	NPB	-inpk	وا در جا <u>جا</u>	Loss plexi	7hr 10mi		dd .	9 5 5	Loss	20r 11mi	ω
2499	_ oo(GPT	_	Per	٠		GPT	_	Pe	٠	
2500	(00			Σ			ş		22		
2501	00 = 10	GPT-npbpe100-sfs 13M	512 4 512 31	Loss: 1.1808 Perplexity: 3.2571	rii och)	_	9	512	Loss: 0.7624 Perplexity: 2.1435	och)	_
2502	NPBPE100 :ab_size = '	bpe, 13M	_embd: 51 n_layer: 4 n_head: 8 lr: 0.0001	:1.1 ity:	7hr 47min 5min/epoc	20min	bpe1	_embd: 51. n_layer: 4 n_head: 2 lr: 0.0001	: 0.7	ır 12 n/ep	27min
2503	NPE cab	-Inp	n_embd: 512 n_layer: 4 n_head: 8 lr: 0.0001	Loss: 1.1808 rplexity: 3.25	7hr 47min (15min/epoch)	7	Ę.	n_embd: 512 n_layer: 4 n_head: 2 lr: 0.0001	Loss: 0.7624 rplexity: 2.14;	1d 2hr 12min (20min/epoch)	7
2504	(vo	GP.	_	Pe			G G	_	Pe		
2505	(0	Įş.		98			ş		32		
2506	NPBPE60 (vocab_size = 60)	GPT-npbpe60-sfs 25.5M	512 : 8 : 8)1	Loss: 0.7269 Perplexity: 2.0686	ch (to	٠Ę	GPT-npbpe60-rds 12.9M	512 : 4 : 8 : 8	Loss: 0.4695 Perplexity: 1.5992	1d 12hr (30min/epoch)	٠Ę
2507	NPBPE60 :ab_size =	pbpe6 25.5M	n_embd: 512 n_layer: 8 n_head: 8 lr: 0.0001	Loss: 0.7269 erplexity: 2.06	2d 4hr 25min (1hr/epoch)	2hr 32min	npbpe6 12.9M	n_embd: 512 n_layer: 4 n_head: 8 lr: 0.0001	Loss: 0.4695 erplexity: 1.59	1d 12hr min/epo	1hr 15min
2508 2509	NP cab	T-nk		Loss	2d 4l (1hr	2hr	두 -	틸리한	Loss	30m	ţ.
2510	٨	<u>p</u>		P			ភ្ជ		Pe		
2511	124)			8					2	_ 🖻	
2512	= 79	GPT-BPE-sfs 33.6M	512 : 8 : 8 01	Loss: 0.7471 Perplexity: 2.1108	2d 6hr 41min (1hr30/epoch)	·듣	GPT-BPE-rds 33.6M	512 : 8 : 8 01	Loss: 0.4770 Perplexity: 1.6112	2d 16hr 26min (1hr15min/epoch)	Æ
2513	BPE_size	1-BPE	n_embd: 512 n_layer: 8 n_head: 8 lr: 0.0001	Loss: 0.7471 erplexity: 2.11	2d 6hr 41min (1hr30/epoch)	3hr 55min	T-BPE- 33.6M	n_embd: 512 n_layer: 8 n_head: 8 lr: 0.0001	Loss: 0.4770 prplexity: 1.61	ihr 2 min/e	3hr 22min
2514	ab	GPT.	و در در ج	Loss	2d 6 11hr3	뚮	3PT	취기기반	Loss	2d 16 hr15	К
2515	(vo			ď					٣	" €	
2516	is (53)			80					89	_	
2517	MILE 10	-sfs	512 : 4 :: 8 01	1.90	1mir ooch	Ë	-rds	512 :: 4 :: 4 01	1.51	r och	. <u>⊑</u>
2518	in-Sl	GPT-AIS-sfs 13.9M	n_embd: 512 n_layer: 4 n_head: 8 lr: 0.0001	Loss: 0.6460 erplexity: 1.90	1d 21hr 51min (50min/epoch)	1hr 11min	GPT-AIS-rds 13.9M	n_embd: 512 n_layer: 4 n_head: 4 lr: 0.0001	Loss: 0.4166 erplexity: 1.51	2d 3hr nin/epo	1hr 8min
2519	Atom-in-SMILES BPE (vocab_size = 7924)	GP.	وا در در ب	Loss: 0.6460 Perplexity: 1.9080	1d 2' (50m	£	GPT	ا در در ب	Loss: 0.4166 Perplexity: 1.5168	2d 3hr (45min/epoch)	=
2520	(vo A			4					4		
2521	rel (48)	_ ا		69	٦ <u>ڊ</u>		s		66	۔ <u>ن</u>	
2522	Character-Level	GPT-Char-sfs 25.5M	n_embd: 512 n_layer: 8.0 n_head: 4.0 lr: 0.0001	Loss: 0.5971 Perplexity: 1.8169	1d 22hr 33min (1hr15min/epoch)	ä	GPT-Char-rds 25.5M	n_embd: 512 n_layer: 8 n_head: 8 lr: 0.0001	Loss: 0.3852 Perplexity: 1.4699	3d 13hr 34min (1hr30min/epoch)	лiг
2523	ıcter -	T-Char- 25.5M	embd: 512 n_layer: 8.0 n_head: 4.0 lr: 0.0001	Loss: 0.5971 erplexity: 1.81	2hr (imin/	4hr 12min	T-Char 25.5M	_embd: 51; n_layer: 8 n_head: 8 lr: 0.0001	s: 0.	3hr (4hr 36min
2524	hara ocak	GPT.	وا حاجا ج	Los	1d 2 hr15	4	GPT.	وا دا دا ج	Los	3d 1	4
2525 2526	ح ٥			ď	Ξ				مَ	Ξ	
2527	<u>v</u>	<u></u>	ters	9	<u> </u>	e e	76	ters	ᅙ	5	e l
2528	Model Details	Model Name/ Size	Best Hyper-Parameters	Test Loss and Perplexity	Total Training Time	Inference Time (10k Molecule Generation)	Model Name/ Size	Best Hyper-Parameters	Test Loss and Perplexity	Total Training Time	Inference Time (10k Molecule Generation)
2529	ē D	del Na Size	Best -Paran	st Loss ar Perplexity	al Trair Time	erence Ti 10k Molecul Generation)	del Na Size	Best -Paran	st Loss ar Perplexity	al Train Time	erence Ti 10k Molecul Generation)
2530	Mod	Ψŏ	урег	Test Pe	Tota	Infer (10 o	Mo	урег	Test Pe	Tot	Infer (10 G
2531			£			_		i			
2532	Data Split			e it					E #		
2533	ata			Scaffold Split					Split		
2534	۵							•			
2535	Model					GPT					
2536	Ψ					<u> </u>					
2537	l	ı									

Figure 30: GPT training details.